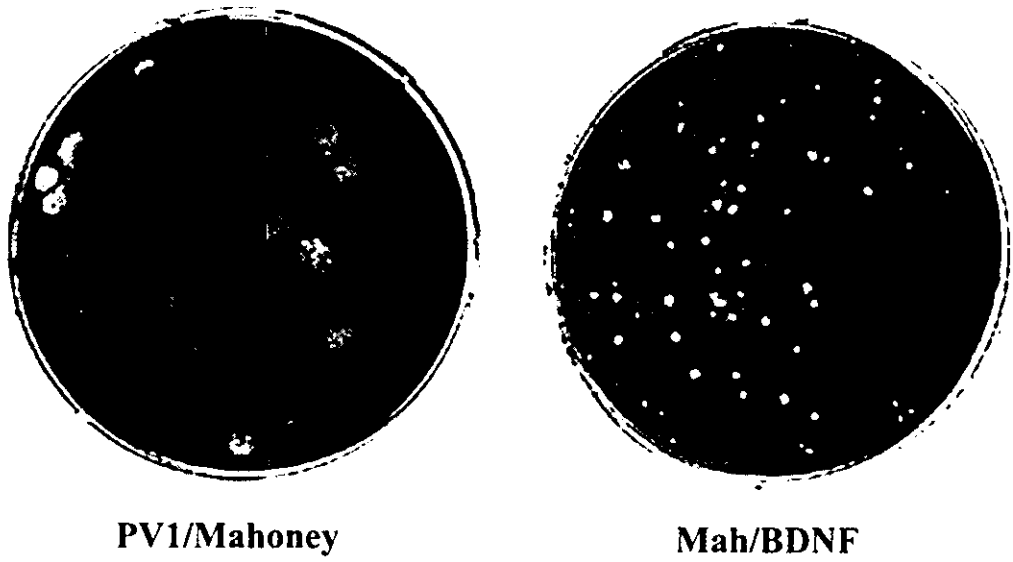

Figure 2 Plaque phenotypes. AGMK cells grown overnight in 60-mm-diameter dishes were infected with PV1/Mahoney or Mah/BDNF. Cells in the dishes were incubated for 72 h at 37°C before being fixed and stained with 1% crystal violet.

PV1/Mahoney in AGMK cells (Figures 2 and 3). The titer of the Mah/BDNF reached only 10% of the wild-type virus at 9 h postinfection (Figure 3).

Because poliovirus, like all other RNA viruses, shows a high rate of genetic variation (Mueller and Wimmer, 1998), foreign sequences, which are dispensable for poliovirus replication, might be deleted rapidly after a few passages in cultured cells. To examine the genetic stability of the Mah/BDNF in cultured cells, the virus recovered from the cells transfected with its RNA was passaged for three more times in AGMK cells. Then, 29 plaques were picked up and the total RNA isolated. RT-PCR was employed to amplify the genome region containing the inserted sequence encoding the mature peptide of BDNF. The bands of intact length (1068 nt) were detected in all the 29 plaque-purified viruses (Figure 4), suggesting that the foreign sequence was stably maintained in the majority of recombinant virus population for up to three passages in the cultured cells. However, the further passage of Mah/BDNF caused appearance of virus population that displayed slightly larger plaques, although the plaque size was much smaller than that of the parental PV1/Mahoney (Figure 5). Based on these observations, all further experiments presented in this report were performed using virus stocks obtained after three passages in AGMK cells.

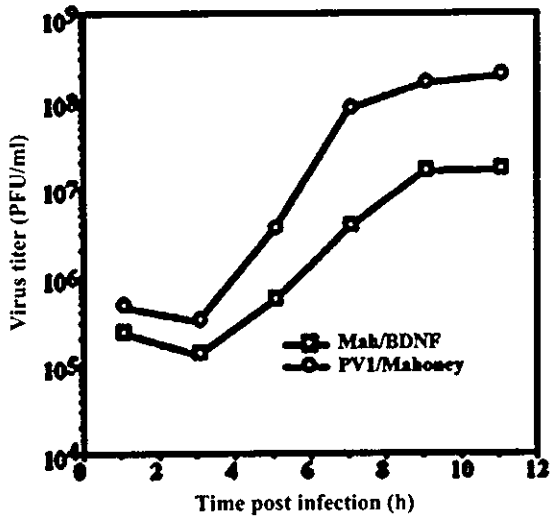

Figure 3 One-step growth curve of polioviruses in cultured cells. AGMK cells grown overnight in 60-mm-diameter dishes at 37°C were infected at an m.o.i. of 10 with PV1/Mahoney or Mah/BDNF obtained after three successive passages in AGMK cells. The cultures were collected at the indicated times. Virus titers were determined by plaque assay.

Expression of BDNF in cultured cells To examine the expression of BDNF by the poliovirus-based vector in cultured cells, AGMK cells were infected with PV1/Mahoney or Mah/BDNF at a multiplicity of infection (m.o.i.) of 10, and then double stained with antibodies against PV1/Mahoney or BDNF. Almost all the cells infected with Mah/BDNF expressed both antigens of PV1/Mahoney and BDNF at 7 h postinfection (Figure 6A–C), suggesting that no significant deletions occurred on the foreign sequence of the recombinant virus genome after three passages of the virus. No expression of BDNF was detected in cells infected with PV1/Mahoney (Figure 6D–F) or mock-infected cells (Figure 6G–I). To further examine the expression of BDNF by Mah/BDNF in cultured cells, Western blot analysis was performed on AGMK cells infected with PV1/Mahoney or Mah/BDNF. Cytoplasmic extracts were prepared at 7 h postinfection and analyzed by immunoblotting as described in Materials and methods. Antibodies to BDNF detected a band with a molecular mass of about 15.2 kDa only in the extracts from Mah/BDNF-infected cells, and not

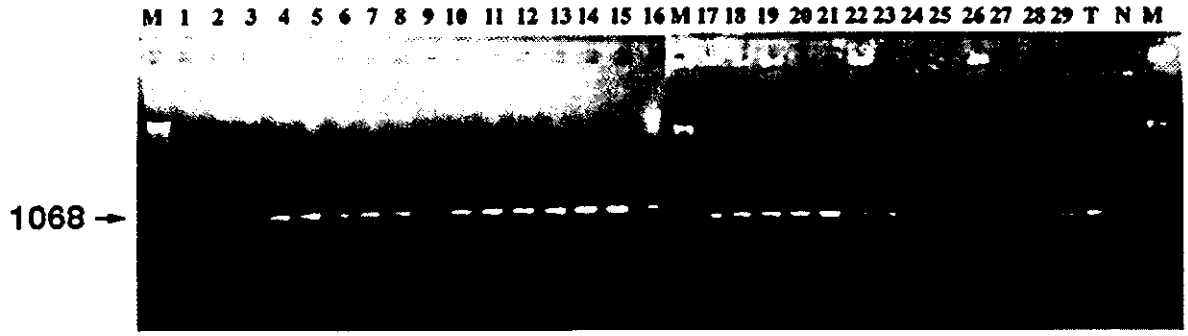

Figure 4 Analysis of the genetic stability of Mah/BDNF in cultured cell. AGMK cells grown in 24-well plates were infected with individual Mah/BDNF isolates obtained after three successive passages in AGMK cells. Total RNAs prepared from the infected cells were subjected to RT-PCR with oligonucleotides 04 and 07 as primers to amplify the genome region that contained the inserted sequence encoding the mature peptide of BDNF. M, DNA molecular weight marker 1KB. T, RNA *in vitro* transcribed from pMah/BDNF. N, RNAs from mock-infected cells as a negative control. Products were analyzed by electrophoresis on a 1% agarose gel. Position of expected RT-PCR product is indicated by an arrow with the length in nucleotides given.

in those from PV1/Mahoney- or mock-infected cells (Figure 7). The 15.2-kDa polypeptide corresponds to the expected molecular mass of BDNF. In addition to the 15.2-kDa band, a 78-kDa band was also detected only in the extracts from Mah/BDNF-infected cells, although the intensity of the 78-kDa band was approximately 10% that of the 15.2-kDa band (data not shown). The 78-kDa band may correspond to unprocessed polyprotein that consists of BDNF (15 kDa), VP0 (37 kDa), and VP3 (26 kDa).

Expression of exogenous BDNF in the central nervous system of transgenic mice Poliovirus is a neurotropic virus, which replicates mainly in the motor neurons of the CNS. Based on this characteristic, we tested whether Mah/BDNF delivers BDNF to the motor neurons of the CNS. Twenty PVR-Tg mice were infected with PV1/Mahoney or Mah/BDNF via an intracerebral inoculation route, and were then observed for up to 4 weeks. All the mice inoculated with 10^6 plaque-forming units (PFU) of PV1/Mahoney died within 7 days, but no mice inoculated with the same amount of Mah/BDNF prepared by three passages developed any paralysis during the observation period. Both exogenous BDNF antigens and PV1/Mahoney antigens were detected in a portion of the neurons from the brains, but no Mah/BDNF-mediated expression of the BDNF was found in the spinal cords (data not shown), of the mice intracerebrally inoculated with Mah/BDNF.

To explore an indirect way of delivering BDNF to the CNS, we injected 10^5 PFU of Mah/BDNF into the quadriceps muscle of PVR-Tg mice, and examined the expression of BDNF and PV1/Mahoney antigens in the lumber spinal cords and brain stems of the mice. Strong expression of the poliovirus antigens was observed in the ventral horn of the lumber cords and some in the dorsal horn from the mice 3 days after the intramuscular injection with Mah/BDNF (Figure 8C). Poliovirus antigens were also detected in the brain stem structures, for example, medial reticular formation, inferior vestibular nucleus, and spinal trigeminal nucleus (Figure 8A). Expression of exogenous BDNF was also detected in motor neurons of the lumber cords (Figure 8D) and in brain-stem neurons (Figure 8B) of these mice. However, both the antigens disappeared in the spinal cords 7 days after the intramuscular inoculation with Mah/BDNF (data not shown). Endogenous BDNF in the spinal cord was detected only in the superficial laminae of the dorsal horn (data not shown). Its presence in the ventral

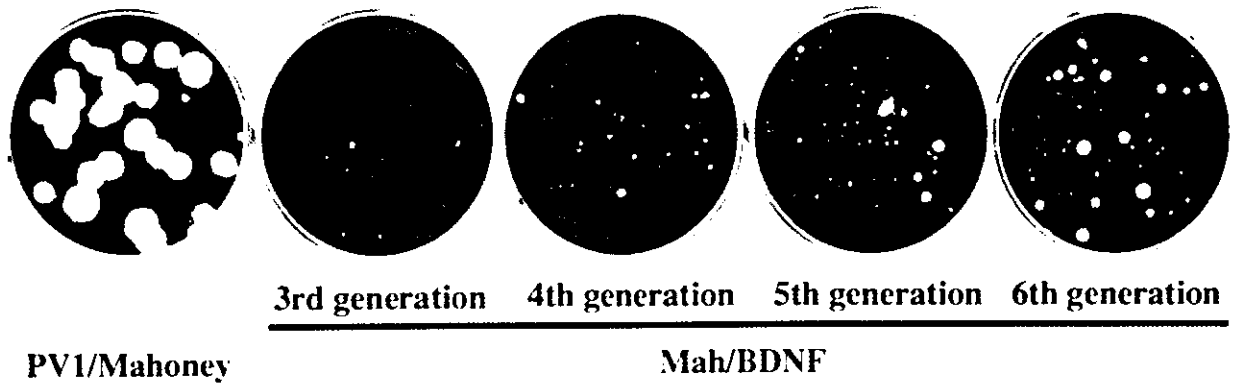

Figure 5 Alteration of plaque phenotypes during passages of Mah/BDNF. PV1/Mahoney, Mah/BDNF preparations of 3rd, 4th, 5th, and 6th generations were used for plaque formation. Other conditions were the same as indicated in the legend to Figure 2.

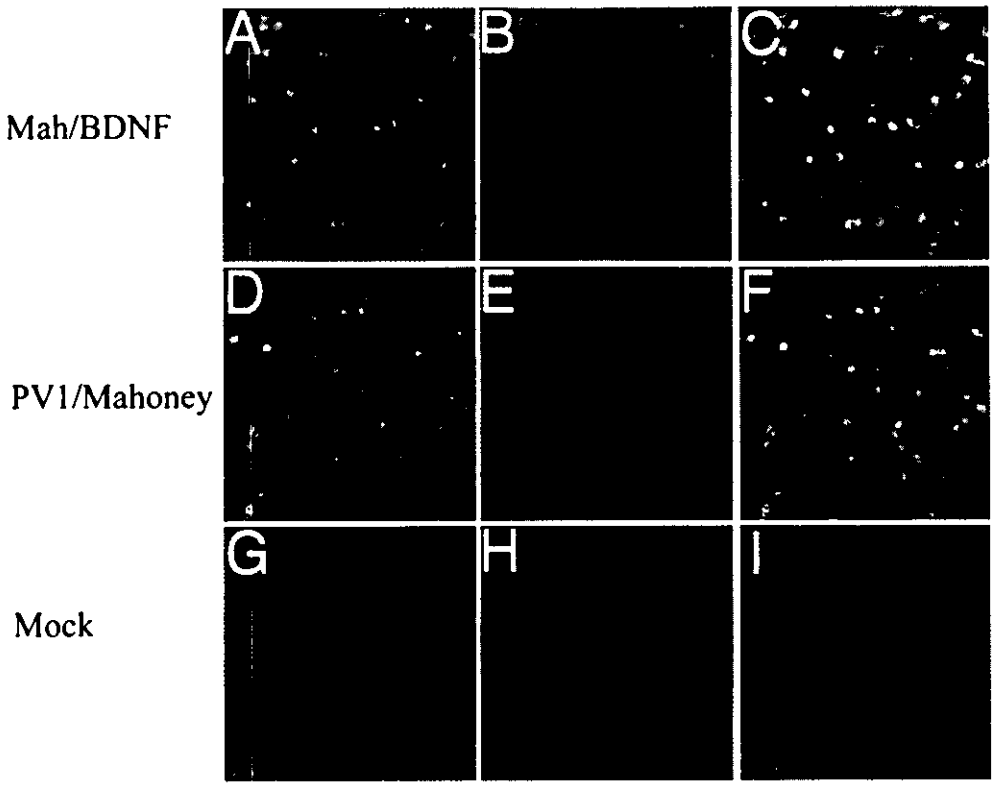

Figure 6 BDNF expression in cultured cells infected with Mah/BDNF. Monolayers of AGMK cells were infected at an m.o.i. of 10 with Mah/BDNF (**A–C**), PV1/Mahoney (**D–F**), or mock-infected with PBS (**G–I**). Cells were fixed and stained as described in Materials and methods. The preparations were visualized with a confocal laser-scanning microscope. PV1/Mahoney antigens (**A**, **D**, and **G**) and BDNF antigens (**B**, **E**, and **H**) are merged in pictures (**C**, **F**, and **I**, respectively).

horn neurons was too sparse to detect by the method used. Motoneuronal cell bodies in the normal and PV1/Mahoney-infected Tg mice were mostly negative in their immunostaining for BDNF.

Replication efficiency of Mah/BDNF in the CNS of PVR-Tg mice We observed that no mouse intracerebrally infected with 10^6 PFU of Mah/BDNF showed any paralysis even 4 weeks after the infection, whereas the LD_{50} of PV1/Mahoney was less than 10^3 PFU. Because efficient replication of poliovirus in the brain of mice appears to be necessary for the virus to cause paralysis (Jia *et al*, 1999), it is possible that Mah/BDNF has an inefficient replicating capacity in the brain as well as in cultured cells (Figures 2 and 3). To test the possibility, we measured virus titers in the brains of PVR-Tg mice infected with 10^4 PFU of PV1/Mahoney or Mah/BDNF (Figure 9). The titer of PV1/Mahoney increased up to 10^8 PFU per brain until 72 h postinfection. However, the titers of Mah/BDNF in the brains increased only to 10^5 PFU per brain at 24 h postinfection, and this level was maintained until 72 h postinfection. This poor replication capacity of Mah/BDNF in the brains of PVR-Tg mice may be a determinant for the decreased neurovirulence of the virus, and may also explain why BDNF antigens were not detected in the spinal cords of mice intracerebrally injected with Mah/BDNF.

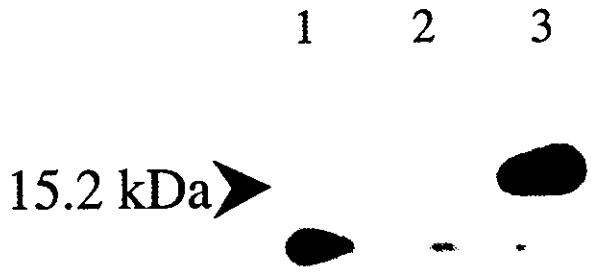

Figure 7 Western blot analysis of BDNF. Cytoplasmic extracts from AGMK cells infected with PV1/Mahoney (lane 2), Mah/BDNF (lane 3), or mock-infected with PBS (lane 1) were analyzed by Western blotting using antibodies against BDNF. Specific bands detected by antibodies against BDNF are indicated by the arrowheads. Four μg of total protein was loaded on each lane.

Discussion

Previous studies have shown that poliovirus in the CNS primarily localizes to motor neurons in the ventral horn of the spinal cord (Bodian, 1949; Ren *et al*, 1990; Koike *et al*, 1991), and that intramuscularly inoculated polioviruses are transported through the axon and cause paralysis in PVR-Tg mice (Ren and Racaniello, 1992; Gromeier and Wimmer, 1998; Ohka *et al*, 1998). Therefore, poliovirus is a promising candidate vector for the gene therapy of motor

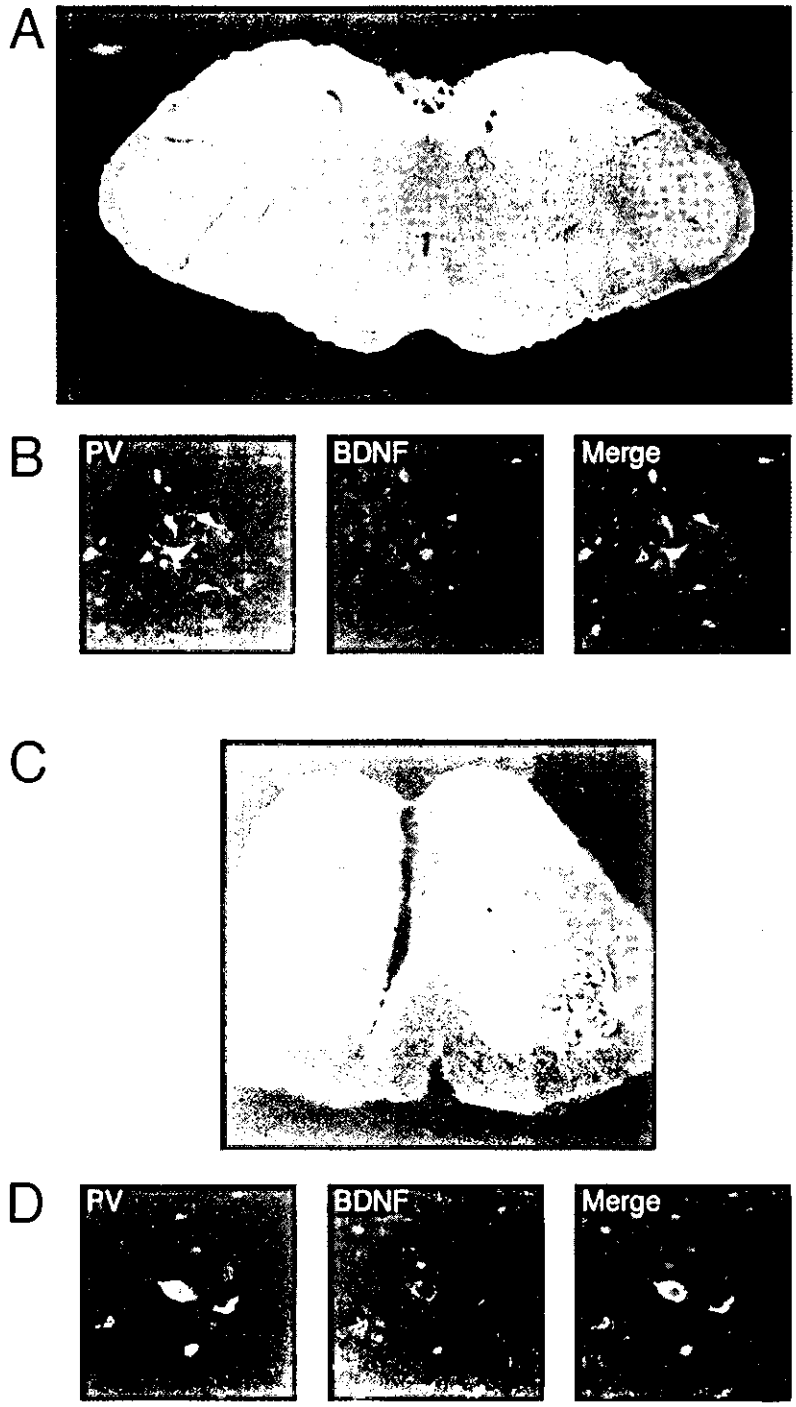

Figure 8 Expression of exogenous BDNF by Mah/BDNF in the CNS of PVR-Tg mice. Three days after the intramuscular inoculation of Mah/BDNF in PVR-Tg mice, poliovirus immunoreactive neurons were detected in the brain stem (**A**) and spinal cord (**C**). Many of poliovirus antigen-positive neurons also expressed BDNF immunoreactivity in their cell bodies, for example, in the brain stem reticular formation (**B**) and spinal lumber cord (**D**).

neuron-related diseases or injuries. BDNF has been reported to prevent motor neuron death in cultures of embryonic motor neurons (Henderson *et al*, 1993; Becker *et al*, 1998). In the case of nerve injury, exogenous BDNF attenuates degeneration and biochemical changes in the affected neurons (Chiu *et al*, 1994; Yan *et al*, 1994). In this report, as a first step toward developing a neurotropic virus vector, we chose poliovirus to express BDNF in the CNS of PVR-Tg mice. PV1/Mahoney, rather than the vaccine virus Sabin 1 strain, was chosen to be the vector to express BDNF because the available strain of PVR-Tg mice does not support the replication of Sabin 1 strain well.

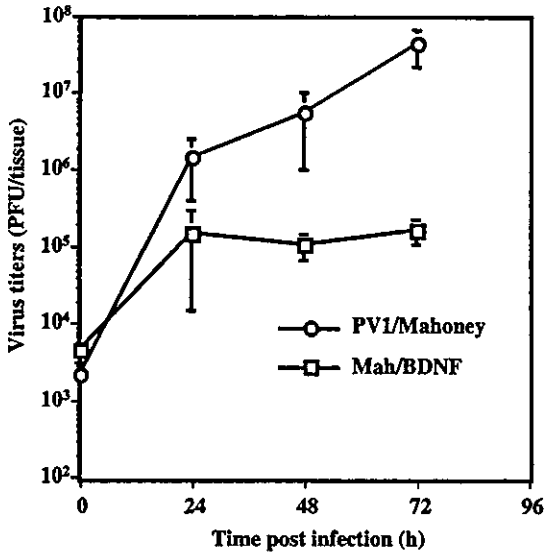

Figure 9 Viral replication in the brains of PVR-Tg mice. PVR-Tg mice were intracerebrally inoculated with 10^4 PFU of PV1/Mahoney (open circle) or Mah/BDNF (open square). Mice were anesthetized and dissected at the indicated times. Virus titers were measured by plaque assays. The values are the means of virus titers obtained from triplicate independent infection experiments. The extent of scattering values is indicated by the vertical lines.

Viral replications of recombinant polioviruses with long foreign nucleotide sequences are severely impaired, and the inserts of more than 700-nt long are usually not stably maintained during passages (Mueller and Wimmer, 1998). However, recombinant polioviruses carrying inserts less than 400-nt long are generally much more stable (Mattion *et al*, 1994, 1995; Tang *et al*, 1997; Yim *et al*, 1996). In this study, BDNF sequence of 423-nt long in the Mah/BDNF genome appeared to be stably maintained until three passages of the virus (Figure 4). Three time-cell passages is enough to prepare virus stocks in practice. However, variants showing larger plaque phenotypes generated during further passages (Figure 5). This may result in difficulties in practical use of poliovirus-based vectors.

When Mah/BDNF was used to infect PVR-Tg mice via an intracerebral inoculation route, none of the mice showed any paralysis. The replication efficiency of Mah/BDNF in the brain was greatly reduced as compared with that of PV1/Mahoney (Figure 9). Furthermore, in PVR-Tg mice intramuscularly inoculated with Mah/BDNF, antigens of BDNF were detected in the motor neurons at 3 days postinfection (Figure 8) but not at 7 days postinfection (data not shown). The poliovirus antigens also disappeared at 7 days postinfection. These results suggest that the foreign sequence encoding BDNF unexpectedly reduced the replication efficiency and therefore lowered the neurovirulence of PV1/Mahoney, although 1 of 12 or 2 of 6 mice developed paralysis after the intramuscular inoculation with 1 of 12; 2×10^4 or 2 of 6; 4×10^5 PFU of Mah/BDNF, respectively (data not shown). Thus, it is clearly necessary to reduce neurovirulence of Mah/BDNF for practical use. By contrast, the observation of short-lived Mah/BDNF in the CNS may be indicative of a relatively safe character of the recombinant. The expression of exogenous BDNF itself may have an ability to reduce poliovirus replication in the CNS, although BDNF showed no effect on poliovirus replication in AGMK cells (data not shown).

Infectious poliovirus replicons, in which the nucleotide sequence encoding the capsid protein (P1) of poliovirus was replaced by the foreign sequence, have been reported to express foreign proteins in the motor neurons of the spinal cords from mice transgenic for the human PVR (Bledsoe *et al*, 2000a, 2000b). The poliovirus replicons do not generate infectious virus particles in the infected cells because no capsid protein is produced, resulting in expression of the foreign gene only in the first target cells. This transient expression system may be safer than that employing replication-competent poliovirus vectors. On the other hand, expression of foreign genes by the former system must be less efficient than the replication-competent one. In any event, both strategies for the expression of foreign genes take advantage of the natural tropism of poliovirus which targets neurons in the CNS, and therefore holds promise for continued development of poliovirus-based vectors for neural gene delivery.

Materials and methods

Cells, viruses, and mice Monolayers of AGMK cells were grown in Dulbecco modified Eagle's medium supplemented with 5% newborn calf serum. They were used for transfections, virus preparations, and plaque assays.

PV1/Mahoney and the recombinant virus Mah/BDNF were recovered from AGMK cells transfected with the corresponding infectious RNA transcripts. The infection of AGMK cells with the recovered virus was regarded as the first passage. Mah/BDNF was amplified for three more times by passaging in AGMK cells at an m.o.i. of 10. The virus titers were determined by plaque assays in AGMK cells. The third generation of Mah/BDNF was used for most experiments.

The transgenic mouse line expressing PVR (CD155) (PVR-Tg mice), ICR-PVRTg21 (Koike *et al*, 1991), at the age of 6 to 10 weeks, was used as an animal model for the infection experiments. All mice used were maintained under specific-pathogen-free conditions.

DNA manipulation All cloning enzymes and reaction buffers were purchased from New England Biolabs or Takara Ltd. Co. (Japan), and used as recommended by the manufacturers.

A poliovirus 5′-proximal portion-based vector was constructed by inserting a synthetic linker which contained the unique *Not*I and *Sac*I sites, coding

sequences of a four-glycine tract and a cleavage recognition site for poliovirus proteinase $3C^{pro}$, at nucleotide position (nt) 746 of pOM, an infectious cDNA clone of PV1/Mahoney (Shiroki *et al*, 1995). This was done by means of PCR using primers 01–02 and 03–04 to amplify the portions of pOM corresponding to nt 1 to 746 and 746 to 1201. The primers 02 and 03 introduced the synthetic linker into the nt 746 of pOM. The two PCR fragments were used as templates for further nucleotide amplification with primers 01 and 04. The 1212-bp *Eco*RI and *Nru*I (nt 1172) fragment was then inserted into the *Eco*RI-*Nru*I sites of the plasmid pBR322 to yield pBR-PV5′(N^+S^+).

A 423-bp nucleotide that included the sequence encoding the mature peptide of rat BDNF (nt 439–819) (Maisonpierre *et al*, 1991) flanked by the *Not*I and *Sac*I restriction sites was amplified from the plasmid pBS-BDNF (kindly provided by EG Jones from University of California at Davis) by PCR using primers 05–06 and then inserted into the *Not*I-*Sac*I sites of pBR-PV5′(N^+S^+) to yield pBR-PV5′BDNF. The AatII fragment of pOM was replaced by the corresponding fragment of pBR-PV5′BDNF to yield pMah/BDNF. The nucleotide sequences of the PCR products and the inserted foreign sequences in the recombinant infectious cDNAs were determined to confirm that no additional mutations occurred and that the inserted sequences were not deleted.

RNA transfection RNA transcripts were synthesized from P*vu*I-linearized infectious cDNAs. AGMK cells in 60-mm-diameter dishes were transfected with 1 to 5 μg of RNA using a DEAE-dextran method (Jia *et al*, 1999). The viruses recovered from the cells transfected with pMah/BDNF were designated Mah/BDNF.

One step growth curve Monolayers of AGMK cells grown in 60-mm-diameter dishes were infected with viruses at an m.o.i. of 10, and incubated at 37°C. Infected cells were collected at the indicated times and lysed by three rounds of freezing and thawing. The cell debris was spun down with a low-speed centrifugation and virus titers (PFU/ml) determined by plaque assays.

RT-PCR AGMK cells were infected at an m.o.i. of 10 with Mah/BDNF obtained after three successive passages in AGMK cells. Total RNAs from the infected cells were prepared by ISOGEN (Nippongene, Fukuyama, Japan)/chloroform extraction 7 h postinfection and precipitated with ethanol according to the instructions of the manufacturer. Reverse transcription (RT) was performed with Superscript™ II RT (Gibco) for 60 min at 37°C using primer 04. After the reaction was completed, the enzyme was inactivated by a 2-min incubation at 95°C. An aliquot (2 μl) of the product was used as a template for the PCR. PCR was performed by using Ex Taq polymerase (Takara, Japan) with primers 07 and 04 to amplify the region of the poliovirus genome that contained the inserted sequence encoding the mature peptide of BDNF.

Immunofluorescence and Western blot analysis Immunofluorescence and Western blot analysis were performed to detect the expression of BDNF in cultured cells infected with Mah/BDNF. For the immunofluorescence assay, AGMK cells grown on 8-well culture slides were infected with PV1/Mahoney or the recombinant Mah/BDNF at an m.o.i. of 10, and then incubated for 7 h at 37°C. The infected cells were washed once with phosphate-buffered saline (PBS) (10 mM phosphate buffer, pH 7.0, 137 mM NaCl, and 2.6 mM KCl), and fixed with 2% paraformaldehyde for 10 min at room temperature. The fixed cells were double stained with a mouse monoclonal antibody against PV1/Mahoney and rabbit polyclonal antibodies against BDNF (Santa Cruz, Biotechnology). They were then subsequently stained with Texas Red-conjugated goat anti-mouse IgG and FITC-conjugated goat anti-rabbit IgG. The preparations were visualized with a confocal laser-scanning microscope (BioRad).

For Western blot analysis, AGMK cells grown in 60-mm-diameter dishes (2×10^6 cells/dish) were infected with PV1/Mahoney or Mah/BDNF at an m.o.i. of 10 and then incubated for 7 h at 37°C. The infected cells were harvested, and lysed in chilled buffer H (10 mM Hepes, pH 7.9, 10 mM KCl, 1.5 mM MgCl, 1 mM DTT, 1% Triton X-100, and 0.1 mM phenymethylsulfonyl fluoride) (Andino *et al*, 1993). The nuclei were removed by a low speed centrifugation. Approximately 4 μg of proteins from the total lysates were subjected to electrophoresis on a 12% polyacrylamide gel containing 0.1% SDS and then analyzed by immunoblotting. The blots were incubated with rabbit polyclonal antibody against BDNF (Santa Cruz, Biotechnology). Horseradish peroxidase-conjugated goat anti-rabbit immunoglobulins and enhanced-chemiluminescence detection kits were purchased from Amersham. The immunoblotting was performed according to the recommendations of the manufacturer.

Infection of PVR-Tg mice with Mah/BDNF and preparation of tissues for immunohistochemistry PVR-Tg mice were anesthetized by intraperitoneal injection with 0.3 to 0.4 ml of ketamine (10 mg/ml) and xylazine (0.2 mg/ml) in PBS. The anesthetized mice were injected with virus suspensions using an intracerebral (10^6 PFU/30 μl/mouse) or intramuscular (10^5 PFU/100 μl/mouse) inoculation route. For the intramuscular inoculation, the virus suspension was injected into quadriceps. The mice were observed daily for up to 4 weeks. At 2, 3, 5, and 7 days postinfection, the mice were anesthetized, perfused with cold 2.5% paraformaldehyde in 0.1 M phosphate buffer (PB) (pH 7.4), and dissected. The tissues were postfixed in the same fixative, and then equilibrated in 0.1 M PB with 30% sucrose. Brains and spinal cords were sectioned at 30-μm thickness using a cryostat and floated in cold 0.1 M PB.

Immunohistochemistry All the reactions were carried out at room temperature, unless otherwise specified. Nonspecific reactions were blocked with

10% normal goat serum. Sections were incubated first with primary rabbit antiserum against PV1/Mahoney overnight at 4°C. After washing in PB, a mixture of Alexa 594-conjugated anti-rabbit IgG (produced in goat) and anti-human BDNF (produced in chicken) antibodies were applied to the sections overnight at 4°C, followed by incubation in 10% normal rabbit serum for 1 h to block excess amount of anti-rabbit IgG. To localize BDNF immunoreactivity, biotinylated anti-chicken IgY (produced in rabbit), avidin-conjugated peroxidase and thyramid solution were used according to the manufacturer's instruction (TSA method, NEN). Between the incubation steps, the sections were extensively washed. Histological examination was carried out with a laser scanning microscope (LSM510, Zeiss).

Virus recovery from the brains of PVR-Tg mice

Mice were intracerebrally infected with 10^4 PFU of viruses and anesthetized as described previuosly. The brains were removed from the mice at the indicated times and homogenized in PBS to prepare 10% tissue emulsions. The emulsions were centrifuged at low speed to remove tissue debris, and the supernatant containing viruses subjected to plaque assay.

Oligonucleotide primers

01 5′CTGAGAATTCGTAATACGACTCACTATAGG TTAAAACAGCTCTGGGG 3′
02 5′TCCTCCTCCTCCGAGCTCTAGGCGGCCGCG CATTATGATACAATTGTC 3′
03 5′CTAGAGCTCGGAGGAGGAGGAGAGGCTTT GTTTCAAGGTGCTCAGGTTTCA 3′
04 5′ATCAGGCAACTTCCACCACC 3′
05 5′AATAGCGGCCGCAACATGTCTATGAGGGTT CG 3′
06 5′CAGGAGCTCTCTTCCCCTTTTAATGG 3′
07 5′TGGCTGCTTATGGTGACAATC 3′

References

Alexander L, Lu HH, Gromeier M, Wimmer E (1994). Dicistronic polioviruses as expression vectors for foreign genes. *AIDS Res Hum Retroviruses* **10(Suppl 2):** S57–S60.

Andino R, Rieckhof GE, Achacoso PL, Baltimore D (1993). Poliovirus RNA synthesis utilizes an RNP complex formed around the 5′-end of viral RNA. *EMBO J* **12:** 3587–3598.

Andino R, Silvera D, Suggett SD, Achacoso PL, Miller CJ, Baltimore D, Feinberg MB (1994). Engineering poliovirus as a vaccine vector for the expression of diverse antigens. *Science* **265:** 1448–1451.

Ansardi DC, Moldoveanu Z, Porter DC, Walker DE, Conry RM, LoBuglio AF, McPherson S, Morrow CD (1994). Characterization of poliovirus replicons encoding carcinoembryonic antigen. *Cancer Res* **54:** 6359–6364.

Barkats M, Bilang-Bleuel A, Buc-Caron MH, Castel-Barthe MN, Corti O, Finiels F, Horellou P, Revah F, Sabate O, Mallet J (1998). Adenovirus in the brain: recent advances of gene therapy for neurodegenerative diseases. *Prog Neurobiol* **55:** 333–341.

Battleman DS, Geller AI, Chao MV (1993). HSV-1 vector-mediated gene transfer of the human nerve growth factor receptor p75hNGFR defines high-affinity NGF binding. *J Neurosci* **13:** 941–951.

Becker E, Soler RM, Yuste VJ, Gine E, Sanz-Rodriguez C, Egea J, Martin-Zanca D, Comella JX (1998). Development of survival responsiveness to brain-derived neurotrophic factor, neurotrophin 3 and neurotrophin 4/5, but not to nerve growth factor, in cultured motoneurons from chick embryo spinal cord. *J Neurosci* **18:** 7903–7911.

Berkemeier LR, Winslow JW, Kaplan DR, Nikolics K, Goeddel DV, Rosenthal A (1991). Neurotrophin-5: a novel neurotrophic factor that activates trk and trkB. *Neuron* **7:** 857–866.

Bledsoe AW, Gillespie GY, Morrow CD (2000a). Targeted foreign gene expression in spinal cord neurons using poliovirus replicons. *J NeuroVirol* **6:** 95–105.

Bledsoe AW, Jackson CA, McPherson S, Morrow CD (2000b). Cytokine production in motor neurons by poliovirus replicon vector gene delivery. *Nat Biotechnol* **18:** 964–969.

Bodian D (1949). Histopathologic basis of clinical findings in poliomyelitis. *Am J Med* **6:** 563–578.

Burke KL, Dunn G, Ferguson M, Minor PD, Almond JW (1988). Antigen chimaeras of poliovirus as potential new vaccines. *Nature* **332:** 81–82.

Chiu AY, Chen EW, Loera S (1994). Distinct neurotrophic responses of axotomized motor neurons to BDNF and CNTF in adult rats. *Neuroreport* **5:** 693–696.

Choi WS, Pal-Ghosh R, Morrow CD (1991). Expression of human immunodeficiency virus type 1 (HIV-1) gag, pol, and env proteins from chimeric HIV-1-poliovirus minireplicons. *J Virol* **65:** 2875–2883.

Crotty S, Lohman BL, Lu FX, Tang S, Miller CJ, Andino R (1999). Mucosal immunization of cynomolgus macaques with two serotypes of live poliovirus vectors expressing simian immunodeficiency virus antigens: stimulation of humoral, mucosal, and cellular immunity. *J Virol* **73:** 9485–9495.

Di Polo A, Aigner LJ, Dunn RJ, Bray GM, Aguayo AJ (1998). Prolonged delivery of brain-derived neurotrophic factor by adenovirus-infected Muller cells temporarily rescues injured retinal ganglion cells. *Proc Natl Acad Sci USA* **95:** 3978–3983.

Eide FF, Lowenstein DH, Reichardt LF (1993). Neurotrophins and their receptors—current concepts and implications for neurologic disease. *Exp Neurol* **121:** 200–214.

Goins WF, Lee KA, Cavalcoli JD, O'Malley ME, DeKosky ST, Fink DJ, Glorioso JC (1999). Herpes simplex virus type 1 vector-mediated expression of nerve growth factor protects dorsal root ganglion neurons from peroxide toxicity. *J Virol* **73:** 519–532.

Goodman JC, Trask TW, Chen SH, Woo SL, Grossman RG, Carey KD, Hubbard GB, Carrier DA, Rajagopalan S, Aguilar-Cordova E, Shine HD (1996). Adenoviral-mediated thymidine kinase gene transfer into the primate brain followed by systemic ganciclovir: pathologic, radiologic, and molecular studies. *Hum Gene Ther* **7:** 1241–1250.

Gromeier M, Wimmer E (1998). Mechanism of injury-provoked poliomyelitis. *J Virol* **72:** 5056–5060.

Haase G, Pettmann B, Vigne E, Castelnau-Ptakhine L, Schmalbruch H, Kahn A (1998). Adenovirus-mediated transfer of the neurotrophin-3 gene into skeletal muscle of pmn mice: therapeutic effects and mechanisms of action. *J Neurol Sci* **160 Suppl 1:** S97–S105.

Henderson CE, Camu W, Mettling C, Gouin A, Poulsen K, Karihaloo M, Rullamas J, Evans T, McMahon SB, Armanini MP, Berkemeier L, Phillips HS, Rosenthal A (1993). Neurotrophins promote motor neuron survival and are present in embryonic limb bud. *Nature* **363:** 266–270.

Hohn A, Leibrock J, Bailey K, Barde YA (1990). Identification and characterization of a novel member of the nerve growth factor/brain-derived neurotrophic factor family. *Nature* **344:** 339–341.

Ip NY, Ibanez CF, Nye SH, McClain J, Jones PF, Gies DR, Belluscio L, Le Beau MM, Espinosa R 3rd, Squinto SP, Persson H, Yancopoulos GD (1992). Mammalian neurotrophin-4: structure, chromosomal localization, tissue distribution, and receptor specificity. *Proc Natl Acad Sci USA* **89:** 3060–3064.

Jia Q, Ohka S, Iwasaki K, Tohyama K, Nomoto A (1999). Isolation and molecular characterization of a poliovirus type 1 mutant that replicates in the spinal cords of mice. *J Virol* **73:** 6041–6047.

Klein RL, Meyer EM, Peel AL, Zolotukhin S, Meyers C, Muzyczka N, King MA (1998). Neuron-specific transduction in the rat septohippocampal or nigrostriatal pathway by recombinant adeno-associated virus vectors. *Exp Neurol* **150:** 183–194.

Koike S, Taya C, Kurata T, Abe S, Ise I, Yonekawa H, Nomoto A (1991). Transgenic mice susceptible to poliovirus. *Proc Natl Acad Sci USA* **88:** 951–955.

Korsching S (1993). The neurotrophic factor concept: a reexamination. *J Neurosci* **13:** 2739–2748.

Leibrock J, Lottspeich F, Hohn A, Hofer M, Hengerer B, Masiakowski P, Thoenen H, Barde YA (1989). Molecular cloning and expression of brain-derived neurotrophic factor. *Nature* **341:** 149–152.

Lewin GR, Barde YA (1996). Physiology of the neurotrophins. *Annu Rev Neurosci* **19:** 289–317.

Liu Y, Kim D, Himes BT, Chow SY, Schallert T, Murray M, Tessler A, Fischer I (1999). Transplants of fibroblasts genetically modified to express BDNF promote regeneration of adult rat rubrospinal axons and recovery of forelimb function. *J Neurosci* **19:** 4370–4387.

Lu HH, Alexander L, Wimmer E (1995). Construction and genetic analysis of dicistronic polioviruses containing open reading frames for epitopes of human immunodeficiency virus type 1 gp120. *J Virol* **69:** 4797–4806.

Maisonpierre PC, Belluscio L, Squinto S, Ip NY, Furth ME, Lindsay RM, Yancopoulos GD (1990). Neurotrophin-3: a neurotrophic factor related to NGF and BDNF. *Science* **247(4949 Pt 1):** 1446–1451.

Maisonpierre PC, Le Beau MM, Espinosa R 3rd, Ip NY, Belluscio L, de la Monte SM, Squinto S, Furth ME, Yancopoulos GD (1991). Human and rat brain-derived neurotrophic factor and neurotrophin-3: gene structures, distributions, and chromosomal localizations. *Genomics* **10:** 558–568.

Mandel RJ, Snyder RO, Leff SE (1999). Recombinant adeno-associated viral vector-mediated glial cell line-derived neurotrophic factor gene transfer protects nigral dopamine neurons after onset of progressive degeneration in a rat model of Parkinson's disease. *Exp Neurol* **160:** 205–214.

Mandl S, Sigal LJ, Rock KL, Andino R (1998). Poliovirus vaccine vectors elicit antigen-specific cytotoxic T cells and protect mice against lethal challenge with malignant melanoma cells expressing a model antigen. *Proc Natl Acad Sci USA* **95:** 8216–8221.

Mattion NM, Reilly PA, Camposano E, Wu SL, DiMichele SJ, Ishizaka ST, Fantini SE, Crowley JC, Weeks-Levy C (1995). Characterization of recombinant polioviruses expressing regions of rotavirus VP4, hepatitis B surface antigen, and herpes simplex virus type 2 glycoprotein D. *J Virol* **69:** 5132–5137.

Mattion NM, Reilly PA, DiMichele SJ, Crowley JC, Weeks-Levy C (1994). Attenuated poliovirus strain as a live vector: expression of regions of rotavirus outer capsid protein VP7 by using recombinant Sabin 3 viruses. *J Virol* **68:** 3925–3933.

Morrow CD, Porter DC, Ansardi DC, Moldoveanu Z, Fultz PN (1994). New approaches for mucosal vaccines for AIDS: encapsidation and serial passages of poliovirus replicons that express HIV-1 proteins on infection. *AIDS Res Hum Retroviruses* **10(Suppl 2):** S61–S66.

Mueller S, Wimmer E (1998). Expression of foreign proteins by poliovirus polyprotein fusion: analysis of genetic stability reveals rapid deletions and formation of cardioviruslike open reading frames. *J Virol* **72:** 20–31.

Ohka S, Yang WX, Terada E, Iwasaki K, Nomoto A (1998). Retrograde transport of intact poliovirus through the axon via the fast transport system. *Virology* **250:** 67–75.

Percy N, Barclay WS, Sullivan M, Almond JW (1992). A poliovirus replicon containing the chloramphenicol acetyltransferase gene can be used to study the replication and encapsidation of poliovirus RNA. *J Virol* **66:** 5040–5046.

Porter DC, Ansardi DC, Morrow CD (1995). Encapsidation of poliovirus replicons encoding the complete human immunodeficiency virus type 1 gag gene by using a complementation system which provides the P1 capsid protein in trans. *J Virol* **69:** 1548–1555.

Ren RB, Costantini F, Gorgacz EJ, Lee JJ, Racaniello VR (1990). Transgenic mice expressing a human poliovirus receptor: a new model for poliomyelitis. *Cell* **63:** 353–362.

Ren R, Racaniello VR (1992). Poliovirus spreads from muscle to the central nervous system by neural pathways. *J Infect Dis* **166:** 747–752.

Shiroki K, Ishii T, Aoki T, Kobashi M, Ohka S, Nomoto A (1995). A new cis-acting element for RNA replication within the 5′ noncoding region of poliovirus type 1 RNA. *J Virol* **69:** 6825–6832.

Tang S, van Rij R, Silvera D, Andino R (1997). Toward a poliovirus-based simian immunodeficiency virus vaccine: correlation between genetic stability and immunogenicity. *J Virol* **71:** 7841–7850.

Yan Q, Matheson C, Lopez OT, Miller JA (1994). The biological responses of axotomized adult motoneurons to brain-derived neurotrophic factor. *J Neurosci* **14:** 5281–5291.

Yim TJ, Tang S, Andino R (1996). Poliovirus recombinants expressing hepatitis B virus antigens elicited a humoral immune response in susceptible mice. *Virology* **218:** 61–70.

THE JOURNAL OF BIOLOGICAL CHEMISTRY
Vol. 277, No. 52, Issue of December 27, pp. 50966–50972, 2002
Printed in U.S.A.

Mitochondrial Localization of Mutant Superoxide Dismutase 1 Triggers Caspase-dependent Cell Death in a Cellular Model of Familial Amyotrophic Lateral Sclerosis*

Received for publication, September 12, 2002
Published, JBC Papers in Press, October 21, 2002, DOI 10.1074/jbc.M209356200

Hideyuki Takeuchi, Yasushi Kobayashi, Shinsuke Ishigaki, Manabu Doyu, and Gen Sobue‡

From the Department of Neurology, Nagoya University Graduate School of Medicine, 65 Tsurumai-cho, Showa-ku, Nagoya 466-8550, Japan

The mutations in superoxide dismutase 1 (SOD1) cause ~20% of familial amyotrophic lateral sclerosis cases. A toxic gain of function has been considered to be the cause of the disease, but its molecular mechanism remains uncertain. To determine whether the subcellular localization of mutant SOD1 is crucial to mutant SOD1-mediated cell death, we produced neuronal cell models with accumulation of SOD1 in each subcellular fraction/organelle, such as the cytosol, nucleus, endoplasmic reticulum, and mitochondria. We showed that the localization of mutant SOD1 in the mitochondria triggered the release of mitochondrial cytochrome *c* followed by the activation of caspase cascade and induced neuronal cell death without cytoplasmic mutant SOD1 aggregate formation. Nuclear and endoplasmic reticulum localization of mutant SOD1 did not induce cell death. These results suggest that the localization of mutant SOD1 in the mitochondria is critical in the pathogenesis of mutant SOD1-associated familial amyotrophic lateral sclerosis.

Amyotrophic lateral sclerosis (ALS)[1] is a paralytic and lethal disease caused by selective death of motor neurons. Approximately 10% of ALS cases occur in familial (FALS) form. The mutations in superoxide dismutase 1 (SOD1) cause ~20% of FALS cases (1, 2), and there is overwhelming evidence of a toxic gain of function as the cause of the disease (3, 4). However, it remains unclear how mutant SOD1 causes the cell death of motor neurons.

Mitochondrial degeneration such as swelling, dilatation, and vacuolation and cytoplasmic aggregate formation containing mutant SOD1 are characteristic pathological features of FALS cases and FALS transgenic mice models with SOD1 mutations (2, 4–9). The major question is where and how mutant SOD1 exerts its toxic function in motor neuron degeneration. In polyglutamine diseases, nuclear localization of mutant proteins with expanded polyglutamine tract is considered an essential process in causing neuronal cell death (10–14). Endoplasmic reticulum (ER) stress by unfolded protein accumulation in the ER is considered to cause familial Alzheimer's disease (15, 16) or autosomal recessive juvenile Parkinsonism (17). These reports suggest that the subcellular localization of mutant or modified protein is crucial to neuronal cell degeneration. In mutant SOD1-associated FALS, many reports have documented that the mitochondria is involved in the pathogenic process (18–26). Moreover, it has been demonstrated that SOD1, considered a cytosolic enzyme, exists in the mitochondria (27–29), suggesting that the mitochondria is the important site in pathogenesis of FALS. On the other hand, it remains controversial as to whether cytoplasmic mutant SOD1 aggregates are toxic (30) or not (31–33). Previous studies have demonstrated that the inhibition of cytoplasmic aggregate formation by heat shock proteins assure cell survival at an early stage but is unable to prevent eventual cell death at the late stage in the *in vitro* models of FALS (34, 35). Thus, it is important to determine in which organelle of the neuron mutant SOD1 triggers neuronal cell death. To examine this issue, we have produced neuronal cell models with the obligatory accumulation of SOD1 in the subcellular fraction/organelle of the cytosol, nucleus, ER, and mitochondria. In the present study, we provided unequivocal evidence that localization of mutant SOD1 in the mitochondria is the primary cause of mutant SOD1-mediated neuronal cell death, triggering the release of mitochondrial cytochrome *c* followed by the activation of caspase cascade. Furthermore, we demonstrated that cytoplasmic mutant SOD1 aggregate formation is independent of mutant SOD1-mediated neuronal cell death.

EXPERIMENTAL PROCEDURES

Plasmid Constructs—The non-organelle-oriented vectors expressing the fusion proteins of human SOD1 (wild type, mutant G93A, and G85R) and enhanced green fluorescent protein (EGFP) were generated with pEGFP-N1 vector (Clontech) as described previously (35). These vectors were designated Cyto-wtSOD1, Cyto-mSOD1^{G93A}, and Cyto-mSOD1^{G85R}, respectively. After these constructs were digested with *Xho*I and *Not*I, EGFP-tagged human SOD1 (wild type, mutant G93A, and G85R) was subcloned into the *Xho*I/*Not*I site of pShooter vectors (pCMV/myc/nuc, pCMV/myc/ER, and pCMV/myc/mito; Invitrogen). The nucleus-oriented vectors with nuclear localizing signals were designated Nuc-wtSOD1, Nuc-mSOD1^{G93A}, and Nuc-mSOD1^{G85R}, respectively. The ER-oriented vectors with ER retention signals were designated ER-wtSOD1, ER-mSOD1^{G93A}, and ER-mSOD1^{G85R}, respectively. The mitochondria-oriented vectors with mitochondrial localizing signals were designated Mito-wtSOD1, Mito-mSOD1^{G93A}, and Mito-mSOD1^{G85R}, respectively. As controls, we used LacZ subcloned into pEGFP-N1 vector or EGFP-tagged LacZ subcloned into pShooter vector. All of the constructs used here were confirmed by DNA sequence analysis.

* This work was supported by grants from the Ministry of Health, Labor and Welfare of Japan and a Center of Excellence grant from the Ministry of Education, Culture, Sports, Science and Technology of Japan. The costs of publication of this article were defrayed in part by the payment of page charges. This article must therefore be hereby marked "*advertisement*" in accordance with 18 U.S.C. Section 1734 solely to indicate this fact.

‡ To whom correspondence should be addressed. Tel.: 81-52-744-2385; Fax: 81-52-744-2384; E-mail: sobueg@med.nagoya-u.ac.jp.

[1] The abbreviations used are: ALS, amyotrophic lateral sclerosis; FALS, familial amyotrophic lateral sclerosis; SOD1, superoxide dismutase 1; ER, endoplasmic reticulum; EGFP, enhanced green fluorescent protein; PI, propidium iodide; TUNEL, terminal deoxynucleotidyltransferase-mediated UTP end labeling; MTS, 3-(4,5-dimethyl-thiazol-2yl)-5-(3-carboxymethoxyphenyl)-2-(4-sulfophenyl)-2H-tetrazolium; PCD, programmed cell death; COX, cytochrome *c* oxidase; AIF, apoptosis-inducing factor; Smac, second mitochondria-derived activator of caspase; ANOVA, analysis of variance.

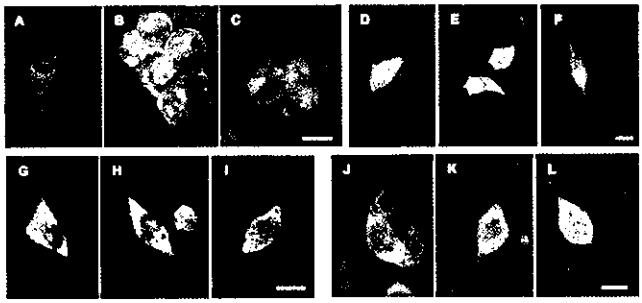

FIG. 1. **Subcellular localization of SOD1-EGFP in Neuro2a cells.** Overlays of two images were taken by laser confocal microscopy 48 h after transfection. *A*, Cyto-wtSOD1; *B*, Cyto-mSOD1^{G93A}; *C*, Cyto-mSOD1^{G85R}; *D*, Nuc-wtSOD1; *E*, Nuc-mSOD1^{G93A}; *F*, Nuc-mSOD1^{G85R}; *G*, ER-wtSOD1; *H*, ER-mSOD1^{G93A}; *I*, ER-mSOD1^{G85R}; *J*, Mito-wtSOD1; *K*, Mito-mSOD1^{G93A}; *L*, Mito-mSOD1^{G85R}. SOD1-EGFP fusion proteins (*green*) were observed comparatively ubiquitous in the cells with Cyto-SOD1 containing no organelle-oriented signals (*A–C*). Only cells with Cyto-mSOD1 contained aggregates of SOD1-EGFP (*B* and *C*). In contrast, each transient expression of organelle-oriented SOD1 (Nuc-, ER-, and Mito-SOD1) was mainly observed in each organelle without aggregate formation regardless wild type or mutant (*D–L*). In cells with Nuc-SOD1, SOD1-EGFP fusion proteins were observed mainly in the nucleus (*D–F*). In the cells with ER-SOD1, SOD1-EGFP fusion proteins were observed mainly in the ER (*G–I*). In the cells with Mito-SOD1, SOD1-EGFP fusion proteins were observed mainly in the mitochondria (*J–L*). The cells were counterstained with propidium iodide (*red*). *Scale bars*, 10 μm.

Cell Culture—Mouse neuroblastoma cell line Neuro2a cells were maintained in Dulbecco's modified Eagle's medium (Invitrogen) supplemented with 10% fetal calf serum (Invitrogen) as described previously (35). They were cultured in Lab-Tec II 4-well chamber slides (Nalge Nunc International) coated with rat tail collagen (Roche Diagnostics). Transient expression of each vector (0.4 μg of DNA/well) in Neuro2a cells (2×10^4 cells/well) was accomplished with LipofectAMINE Plus reagent (Invitrogen). After a 3-h incubation with transfection reagents, the transfected cells were cultured in differentiation medium (Dulbecco's modified Eagle's medium supplemented with 1% fetal calf serum and 20 μM retinoic acid). For treatment with the broad caspase inhibitor (zVAD-fmk; Promega) and the caspase-9-specific inhibitor (zLEHD-fmk; Calbiochem), either 20 μM zVAD-fmk or 20 μM zLEHD-fmk was added at this time.

Cell Fractionation—At each time point (12, 24, and 48 h) after transfection, the cells were collected and gently homogenized with a Dounce homogenizer in cold buffer (250 mM sucrose, 10 mM Tris-HCl, pH 7.5, 5 mM $MgCl_2$, 2 mM EDTA, and protease inhibitor mixture (Complete Mini EDTA-free; Roche Diagnostics)). The homogenates were centrifuged (600 × *g*, 10 min), and the pellets were designated as the nuclear fractions. The supernatants were centrifuged (10,000 × *g*, 10 min), and the resulting pellets were designated as the mitochondrial fractions. The supernatants were centrifuged (100,000 × *g*, 60 min), and the resulting pellets were designated as the microsomal fractions. The supernatants were centrifuged (300,000 × *g*, 60 min), and the resulting supernatants were designated as the cytosolic fractions. Each pellet was resuspended in TNES buffer (50 mM Tris-HCl, pH 7.5, 150 mM NaCl, 1% Nonidet P-40, 2 mM EDTA, 0.1% SDS, and protease inhibitor mixture (Complete Mini EDTA-free; Roche Diagnostics)). The insoluble debris was briefly pelleted. To verify the fractionation, each fraction was subjected to Western blotting for Sp1 as a nuclear marker using anti-Sp1 rabbit polyclonal antibody (1:1,000, Santa Cruz), cytochrome *c* oxidase (COX) as a mitochondrial marker using a anti-COX subunit IV mouse monoclonal antibody (1:1,000; Molecular Probes), GRP78 as a microsomal marker using anti-GRP78 goat polyclonal antibody (1:1,000; Santa Cruz), and β-actin as a cytosolic marker using anti-β-actin mouse monoclonal antibody (1:5,000; Sigma).

Western Blot Analysis—The protein concentration was determined with a DC protein assay kit (Bio-Rad), and Western blotting was processed as described previously (35). To verify the subcellular localization of SOD1-EGFP fusion proteins, 20 μg of protein from each fraction was loaded. For analyzing the release of cytochrome *c*, apoptosis-inducing factor (AIF), and second mitochondria-derived activator of caspase (Smac) from the mitochondria into the cytosol and for analyzing the translocation of Bax, Bak, Bid, Bad, and Bim from the cytosol into the mitochondria, 20 μg of protein from the mitochondrial fraction or the cytosolic fraction was loaded, and the cells incubated with 10 nM staurosporin for 24 h served as a positive control.

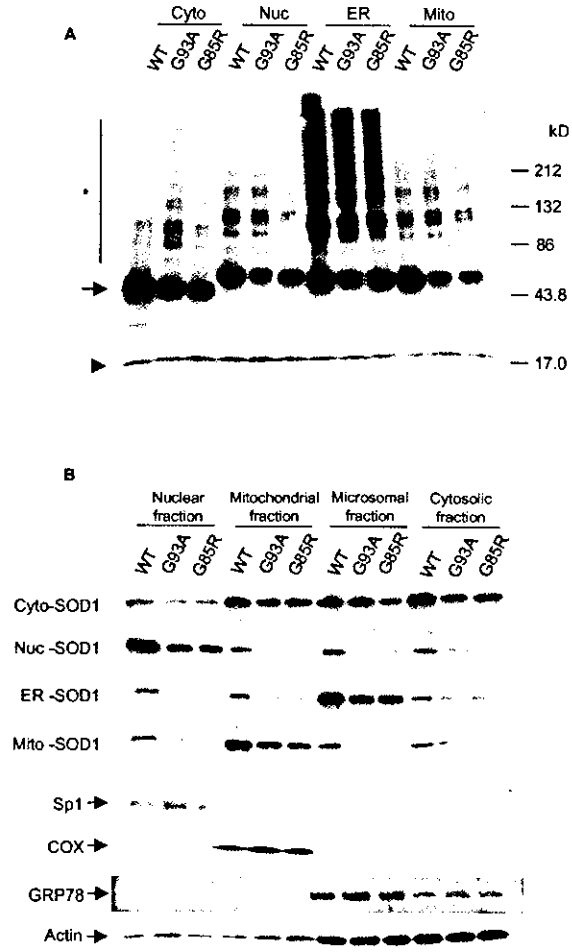

FIG. 2. **Protein level of SOD1-EGFP fusion proteins analyzed by Western blots.** To each well, 20 μg of protein of the sample was applied. *WT*, wtSOD1; *G93A*, mSOD1^{G93A}; *G85R*, mSOD1^{G85R}. *A*, protein levels of SOD1-EGFP fusion proteins 48 h after transfection. The protein level of SOD1-EGFP fusion protein (*arrow*) was much higher than endogenous SOD1 (*arrowhead*). The protein level of the mutant SOD1-EGFP was consistently less than that of wild type SOD1-EGFP regardless of vector type. SOD1 immunoreactive, ladder-like, slowly migrating masses speculated to be SOD1-EGFP oligomers were observed through the gels (*asterisk*), but no significant difference was recognized in the lanes between wtSOD1 and mSOD1. *B*, subcellular localization of SOD1-EGFP fusion proteins 48 h after transfection. Transient expression of SOD1-EGFP fusion protein by Cyto-SOD1 vectors was observed to be comparatively ubiquitous in each cell fraction (*top panel*). In contrast, each transient expression of SOD1-FGFP by organelle-oriented vectors (Nuc-, ER-, and Mito-SOD1) was observed in each organelle (*second*, *third*, and *fourth panels*, respectively.). Sp1, COX, GRP78, and β-actin were used as markers of the nuclear, mitochondrial, microsomal, and cytosolic fraction, respectively.

To assess the protein levels of SOD1-EGFP fusion proteins and the activation of caspase-9 and -3, cells were collected at each time point (12, 24, and 48 h) after transfection and lysed in TNES buffer. Insoluble debris was pelleted, and 20 μg of protein was loaded.

The primary antibodies used here were as follows: anti-SOD1 rabbit polyclonal antibody (1:10,000; StressGen Biotechnologies), anti-caspase-3 rabbit polyclonal antibody, anti-caspase-9 rabbit polyclonal antibody (1:1,000; Cell Signaling), anti-cytochrome *c* mouse monoclonal antibody (1:1,000; BD PharMingen), anti-AIF rabbit polyclonal antibody, anti-Smac goat polyclonal antibody (1:500; Santa Cruz Biotechnology), anti-Bax rabbit polyclonal antibody, anti-Bak rabbit polyclonal antibody, anti-Bad rabbit polyclonal antibody, anti-Bid rabbit polyclonal antibody, and anti-Bim goat polyclonal antibody (1:200; Santa Cruz Biotechnology). After overnight incubation with primary antibodies at 4 °C, each blot was probed with horseradish peroxidase-conjugated anti-rabbit IgG, anti-mouse IgG (1:5,000; Amersham Biosciences) or anti-goat IgG (1:5,000; Santa Cruz Biotechnology). Then they were

visualized with ECL Plus Western blotting detection reagents (Amersham Biosciences). The signal intensity was quantified by densitometry using NIH Image 1.59 software.

Quantitative Assessment of Cytoplasmic Aggregates, Mitochondrial Impairment, and Cell Death—At each time point (12, 24, and 48 h) after transfection, the cells were fixed with 4% paraformaldehyde for 15 min on ice and then permeabilized with 0.05% Triton X-100 at room temperature for 10 min. Next, they were counterstained with 2 μg/ml propidium iodide (PI; Molecular Probes) at room temperature for 10 min and mounted in Gelvatol. A laser confocal scan microscope (MRC1024, Bio-Rad) was used for the morphological analysis, quantitative assessment of aggregates and mitochondrial membrane potentials, and terminal deoxynucleotidyltransferase-mediated UTP end labeling (TUNEL) assay.

For quantitative assessment of aggregates, more than 200 transfected cells in duplicate slides were assessed blindly in three independent trials. The ratio of aggregate-positive cells was calculated as a percentage of such cells among EGFP-positive cells as described previously (25, 35).

For assessment of mitochondrial membrane potential, we used 5,5′,6,6′-tetrachloro-1,1′,3,3′-tetraethylbenzimidazolocarbocyanine iodide (JC-1; Molecular Probes) according to the manufacturer's protocol at each time point (12, 24, and 48 h) after transfection. More than 200 transfected cells in duplicate slides were assessed blindly in three independent trials.

For TUNEL assay, we used the *in situ* cell death detection kit, TMR red (Roche Diagnostics). At each time point (12, 24, and 48 h) after transfection, the TUNEL assay was carried out according to the manufacturer's protocol. As a positive control, we used the EGFP-LacZ transfected cells that were incubated with 10 nM staurosporin for 24 h. More than 200 transfected cells in duplicate slides were assessed blindly in three independent trials.

Cell death was assessed by the dye exclusion method with PI as described previously (25, 35). At each time point (12, 24, and 48 h) after transfection, the cells were incubated with 2 μg/ml PI in Dulbecco's modified Eagle's medium for 15 min at 37 °C and mounted in Gelvatol. More than 200 transfected cells in duplicate slides were assessed blindly in three independent trials under a conventional fluorescent microscope. The ratio of dead cells was calculated as a percentage of PI-positive cells among EGFP-positive cells.

For assessment of cell viability through mitochondrial impairment, we used the 3-(4,5-dimethyl-thiazol-2yl)-5-(3-carboxymethoxyphenyl)-2-(4-sulfophenyl)-2H-tetrazolium (MTS) assay with CellTiter 96 Aqueous one solution assay (Promega). At each time point (12, 24, and 48 h) after transfection, MTS assays were carried out in six independent trials. Absorbance at 490 nm was measured in a multiple plate reader as described previously (13, 25).

Statistical Analysis—All of the results were analyzed by two-way analysis of variance (ANOVA) with Tukey-Kramer post-hoc test using Statview software version 5 (SAS Institute Inc.).

RESULTS

Mito-mSOD1 Induces Significant Cell Death with Lack of Aggregate Formation—Laser confocal microscopic images and Western blots demonstrated that the subcellular localization of SOD1-EGFP fusion proteins expressed by Cyto-SOD1 was comparatively ubiquitous among the subcellular fractions (Figs. 1, *A–C*, and 2*B*). In contrast, each transient expression of organelle-oriented SOD1 (Nuc-, ER-, and Mito-SOD1) was mainly observed in each organelle (Figs. 1, *D–L*, and 2*B*). The protein level of SOD1-EGFP fusion proteins was much higher than endogenous SOD1 (Fig. 2*A*). The protein level of the mutant SOD1-EGFP was consistently less than that of wild type SOD1-EGFP (Fig. 2*A*). As reported previously (32, 35, 36), SOD1 immunoreactive, ladder-like, slowly migrating masses speculated as SOD1-EGFP oligomers were observed through the gels (Fig. 2*A*, *asterisk*), but no constant relation was presented between wtSOD1 and mSOD1 of all vectors. These ladder-like masses were most clearly observed in the lanes of ER-SOD1s, especially ER-wtSOD1 (Fig. 2*A*).

As we previously demonstrated (35), the cells with Cyto-mSOD1 developed cell death and cytoplasmic aggregates of SOD1-EGFP fusion proteins, whereas those with Cyto-wtSOD1 did not (Figs. 1, *A–C*, and 3). The cells with Mito-mSOD1

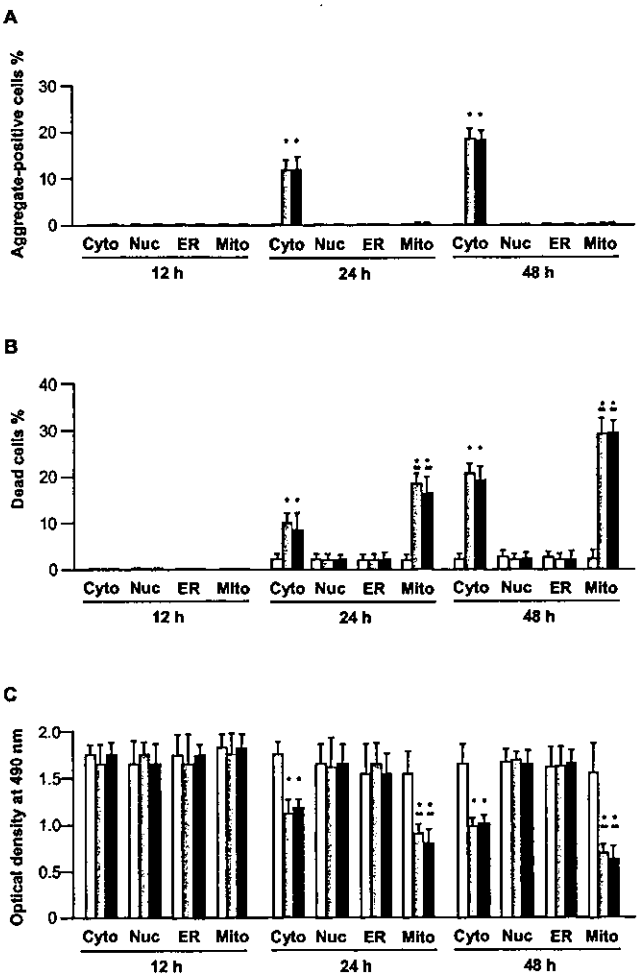

FIG. 3. **Frequency of aggregate-positive cells and dead cells and MTS assay.** *A*, frequency of aggregate-positive cells. *B*, frequency of dead cells. *C*, MTS assay. *White columns*, wtSOD1; *gray columns*, mSOD1^{G93A}; *black columns*, mSOD1^{G85R}; *Cyto*, Cyto-SOD1; *Nuc*, Nuc-SOD1; *ER*, ER-SOD1; *Mito*, Mito-SOD1. *, $p < 0.001$ *versus* wtSOD1 of each vector; **, $p < 0.05$ *versus* Cyto-mSOD1 (by two-way ANOVA with Tukey-Kramer post-hoc test). The values are the means ± S.D. ($n = 6$).

exhibited a more significant level of cell death and mitochondrial impairment than those with Cyto-mSOD1 but did not develop cytoplasmic aggregates (Figs. 1, *K* and *L*, and 3). The cells with Nuc-wt and mSOD1, ER-wt and mSOD1, or Mito-wtSOD1 did not develop cytoplasmic aggregates or show cell death (Figs. 1, *D–J*, and 3). Expression of either the empty vector or the control vector alone did not induce cytoplasmic aggregates and cell death (data not shown). These findings suggest that the localization of mSOD1 in the mitochondria plays a critical role in mSOD1-mediated cytotoxicity, whereas cytoplasmic aggregate formation or oligomeric formation does not. Furthermore, Cyto-mSOD1-induced cell death, which was less significant than Mito-mSOD1-induced cell death, could be mediated by mitochondrial localization of mSOD1 because a moderate amount of mSOD1 was present in the mitochondria.

Mito-mSOD1 Induces Mitochondrial Cytochrome c Release Followed by Sequential Activation of Caspase-9 and -3—We assessed which mitochondrial death signal was involved in mSOD1-mediated cytotoxicity. Western blots revealed that cytochrome *c* release from the mitochondria into the cytosol occurred in the cells with Mito-mSOD1 (Fig. 4*A*). The cells with Cyto-mSOD1 also elicited less cytochrome *c* release (Fig. 4*A*), whereas it did not occur in the cells with Nuc-mSOD1 or ER-mSOD1 (data not shown). The time course of densitometric analysis revealed that the cytochrome *c* release in the cells

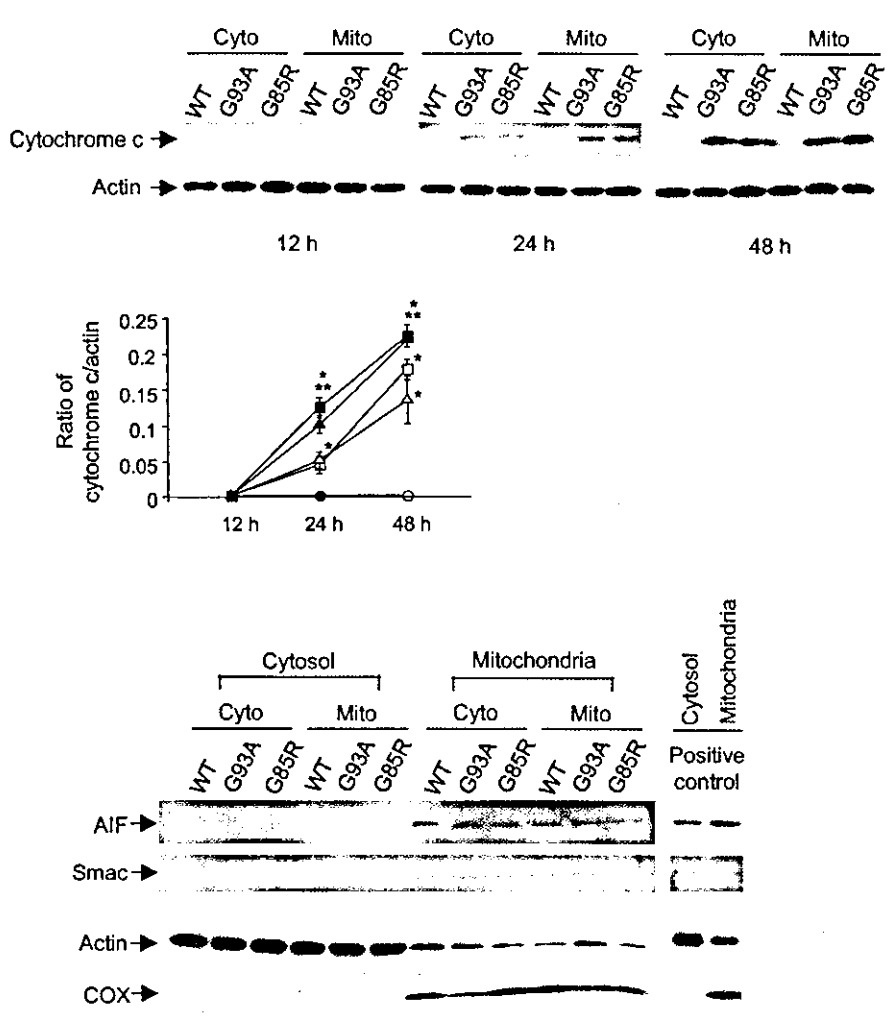

FIG. 4. **Western blot analysis of cytochrome *c*, AIF, and Smac.** *A*, time course of the mitochondrial cytochrome *c* release into the cytosol. *B*, densitometric analysis of cytochrome *c* release. *C*, subcellular localization of AIF and Smac 48 h after transfection. COX and β-actin were used as markers of the mitochondrial and cytosolic fraction, respectively. *WT*, wt-SOD1; *G93A*, mSOD1^{G93A}; *G85R*, mSOD1^{G85R}; *Cyto*, Cyto-SOD1; *Mito*, Mito-SOD1. ○, Cyto-wtSOD1; △, Cyto-mSOD1^{G93A}; □, Cyto-mSOD1^{G85R}; ●, Mito-wtSOD1; ▲, Mito-mSOD1^{G93A}; ■, Mito-mSOD1^{G85R}. *, $p < 0.001$ *versus* wt-SOD1 of each vector; **, $p < 0.05$ *versus* Cyto-mSOD1 (by two-way ANOVA with Tukey-Kramer post-hoc test). The values are the means ± S.D. ($n = 3$).

with Mito-mSOD1 increased gradually and was significantly stronger than those with Cyto-mSOD1 (Fig. 4*B*). Because AIF and Smac are also known as the signal proteins released from the mitochondria into the cytosol that promote apoptosis (37, 38), we examined the release of these mitochondrial proteins into the cytosol in this model. Western blots were not able to detect the release of AIF and Smac in the cells with either Cyto-mSOD1 or Mito-mSOD1 (Fig. 4*C*). Thus, AIF and Smac did not seem to be involved in the neuronal cell death in our model.

Then we examined the downstream signal cascade of the activation of caspase-9 and -3 following the mitochondrial cytochrome *c* release. Western blots demonstrated that the caspase-9 and -3 were activated in the cells with Cyto-mSOD1 and those with Mito-mSOD1, whereas they were not activated in the cells with Cyto-wtSOD1 and those with Mito-wtSOD1 (Fig. 5*A*, *lanes 1–18*). The time course of densitometric analysis revealed that caspase-9 and -3 were activated gradually and sequentially, and both activations were significantly stronger in the cells with Mito-mSOD1 than those with Cyto-mSOD1 (Fig. 5, *B* and *C*).

Bcl-2 Family Pro-apoptotic Proteins Are Not Involved in Cyto-mSOD1 and Mito-mSOD1-induced Cell Death—Bcl-2 family pro-apoptotic proteins such as Bax, Bak, Bid, Bad, and Bim were considered to be translocated from the cytosol to the mitochondria during apoptosis and to promote the mitochondrial cytochrome *c* release to the cytosol (37–39). Thus, we examined whether Bax, Bak, Bid, Bad, and Bim were involved in the cytochrome *c* release in this model. Western blots, however, did not show the translocation of these proteins to the mitochondria (Fig. 5*D*). We also assessed the alteration of mitochondrial membrane potential with JC-1 but were unable to detect a significant difference in the ratio of JC-1 monomer and J aggregates between the cells with wtSOD1 and those with mSOD1 of any vectors (data not shown). These data suggested that mitochondrial localization of mutant SOD1 elicited cytochrome *c* release from the mitochondria to the cytosol followed by caspase activation without involvement of Bcl-2 family pro-apoptotic protein translocation and mitochondrial membrane potential alterations.

Caspase-9-specific Inhibitor and Broad Caspase Inhibitor Prevented Mitochondrial-localized Mutant SOD1-mediated Cell Death—To determine whether the mitochondrial-dependent caspase cascade activation plays a role in the mSOD1-mediated cell death, we examined the effect of treatments with the broad caspase inhibitor (zVAD-fmk) and the caspase-9-specific inhibitor (zLEHD-fmk). Western blots indicated that treatment with 20 μM zVAD-fmk or 20 μM zLEHD-fmk completely blocked the activation of caspase-9 and -3 (Fig. 5*A*, *lanes 19–30*) and diminished mSOD1-mediated cell death and mitochondrial impairment (Fig. 6) in the cells with Mito-mSOD1 as well as Cyto-mSOD1. No significant difference was observed in the inhibitory effect of zVAD-fmk and zLEHD-fmk (Fig. 6). These findings suggest that the pathway from release of cytochrome *c* to activation of caspase-9 and caspase-3 is the main process of mSOD1-mediated neuronal cell death.

Despite the activation of caspase-3, the cells with Cyto-mSOD1 or Mito-mSOD1 showed TUNEL-negative staining as

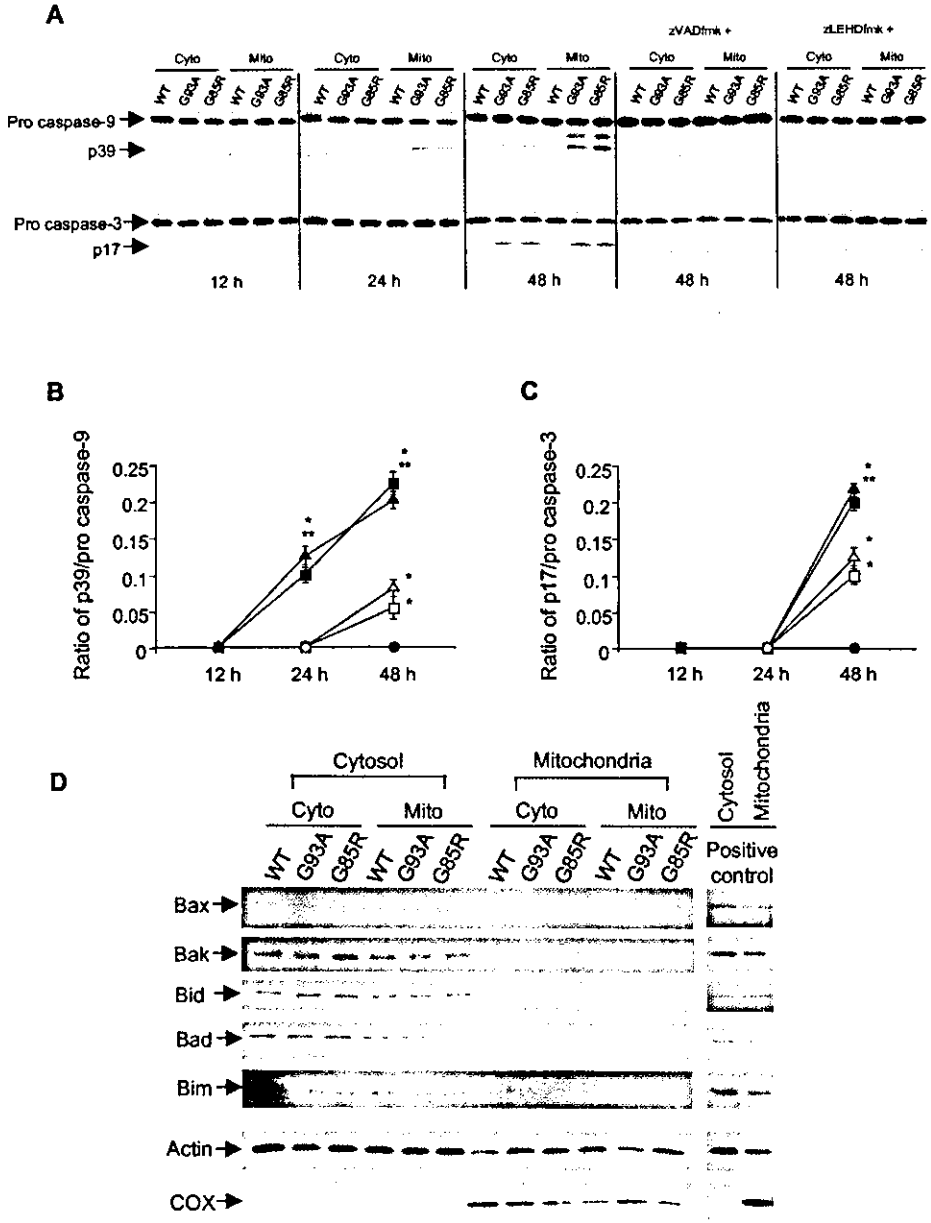

FIG. 5. **Western blot analysis of caspase-9 and -3 and Bcl-2 family pro-apoptotic proteins.** *A*, time course of the activation of caspase-9 and -3. *B*, densitometric analysis of caspase-9 activation. *C*, densitometric analysis of caspase-3 activation. *D*, subcellular localization of Bcl-2 family pro-apoptotic proteins 48 h after transfection. COX and β-actin were used as markers of the mitochondrial and cytosolic fraction, respectively. *WT*, wtSOD1; *G93A*, mSOD1^{G93A}; *G85R*, mSOD1^{G85R}; *Cyto*, Cyto-SOD1; *Mito*, Mito-SOD1. ○, Cyto-wtSOD1; △, Cyto-mSOD1^{G93A}; □, Cyto-mSOD1^{G85R}; ●, Mito-wtSOD1; ▲, Mito-mSOD1^{G93A}; ■, Mito-mSOD1^{G85R}. *, $p < 0.001$ *versus* wt-SOD1 of each vector; **, $p < 0.05$; *versus* Cyto-mSOD1 (by two-way ANOVA with Tukey-Kramer post-hoc test). The values are the means ± S.D. ($n = 3$).

well as those with Cyto-wtSOD1 or Mito-wtSOD1 (Fig. 7, *A–F*), whereas cells treated with staurosporin exhibited obvious TUNEL-positive staining and nuclear pycnosis (Fig. 7, *G–I*).

DISCUSSION

Here we provided unequivocal evidence that mitochondrial localization of mutant SOD1 is the essential part of mutant SOD1-mediated neurotoxicity in a cellular model of FALS. First, neuronal cell death was elicited when mutant SOD1 was localized in the mitochondria, not in the nucleus nor ER, and was not associated with cytoplasmic aggregate formation. Second, the extent of cytochrome *c* release and following caspase-9 and -3 activation were markedly enhanced by accumulation of mutant SOD1 in the mitochondria. Third, Bcl-2 family pro-apoptotic proteins such as Bax, Bak, Bid, Bad, and Bim and the mitochondrial membrane potential alterations were not involved in the cytochrome *c* release from the mitochondria into the cytosol in our model. Fourth, a caspase-9-specific inhibitor zLEHD-fmk as well as a broad caspase inhibitor zVAD-fmk diminished mutant SOD1-mediated neuronal cell death. Thus, the localization of mutant SOD1 in the mitochondria triggers the cytochrome *c* release followed by caspase-dependent neuronal cell death independent of Bcl-2 family pro-apoptotic proteins and alteration of mitochondrial membrane potentials. Furthermore, mutant SOD1-mediated cell death was independent of cytoplasmic aggregate formation. A previous study reported that Bax translocation from the cytosol to the mitochondria was associated with cytochrome *c* release from the mitochondria into the cytosol in the FALS transgenic mice model (20), but there is a possibility that the surroundings of motor neurons such as astorocytes or dying neurons might affect Bax translocation in the model used.

Mitochondrial involvement in ALS and FALS has been documented (18–26). Mitochondrial degeneration of vacuolation or membrane disintegration in motor neurons is one of the earliest pathological findings in FALS transgenic mice (2, 5, 8, 9). Moreover, mitochondrial dysfunctions such as altered calcium homeostasis (18), decrease in respiratory chain complex activity (22, 23), alteration of the mitochondria-related gene expression (24), and increase in reactive oxygen species (39) have been reported in *in vitro* and *in vivo* models. Recent studies revealed that SOD1, which has been considered to be a cytosolic enzyme, also exists in the mitochondria (25–27) and that

mutant SOD1 was present in the vacuolated mitochondria of FALS transgenic mice model (27). Previous studies also revealed that cytochrome *c* release and subsequent caspase activation occurred (20, 21, 25, 40–43) and that inhibition of cytochrome *c* release by minocycline (21), coexpression of X chromosome-linked inhibitor of apoptosis protein (25), and treatment with a broad caspase inhibitor zVAD-fmk (42) inhibited cell death in the *in vitro* and *in vivo* models of FALS. In this study, we unequivocally demonstrated that mitochondrial localization of mutant SOD1 itself is primary and crucial to elicit the following mitochondrial death signals for mutant SOD1-mediated neuronal cell death. The cells with Cyto-mSOD1 showed a lesser extent of cell death than those with Mito-SOD1, probably because mutant SOD1 by Cyto-mSOD1 accumulated less in the mitochondria than that by Mito-SOD1.

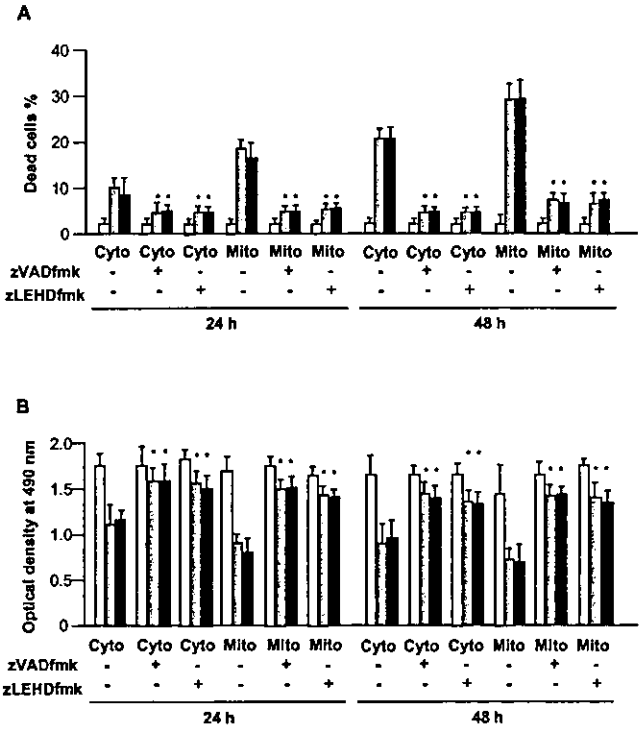

FIG. 6. **Frequency of dead cells and MTS assay after treatment with caspase inhibitors.** *A*, frequency of dead cells. *B*, MTS assay. *White columns*, wtSOD1; *gray columns*, mSOD1^{G93A}; *black columns*, mSOD1^{G85R}; *Cyto*, Cyto-SOD1; *Mito*, Mito-SOD1. *, $p < 0.001$ *versus* untreated mSOD1 of each vector (by two-way ANOVA with Tukey-Kramer post-hoc test). The values are the means ± S.D. ($n = 6$).

In the present study, similar to previous reports (32, 35, 36), SOD1 immunoreactive, ladder-like, slowly migrating masses speculated to be SOD1-EGFP oligomers were observed on Western blots (Fig. 2*A*, *asterisk*), but no significant difference was detected between wtSOD1 and mSOD1 of all vectors. These ladder-like masses were most clearly observed in the ER-SOD1s, probably because SOD1-EGFP fusion proteins with ER retention signals may avoid proteasome-mediated degradation and tend to accumulate in the ER as an unfolded form. The level of these ladder-like, slowly migrating masses was not associated with neuronal cell death, but there remains the possibility that localization of mutant SOD1 oligomers in the mitochondria may cause neurotoxicity. The mitochondrial quality control system depends on ATP-dependent protease complexes such as homologues of Lon and Hsp70 (44–46). However, the capacity of mitochondria to deal with abnormal proteins might be rather limited, and the mitochondria seem to release death signals when abnormal proteins overflowed. Further investigations are needed to give an answer to this issue.

Cytoplasmic aggregate formation containing mutant SOD1 is a hallmark of mutant SOD1-associated FALS, and it has been demonstrated in the *in vitro* and *in vivo* FALS models (2, 4–9). These aggregates have been considered to participate in

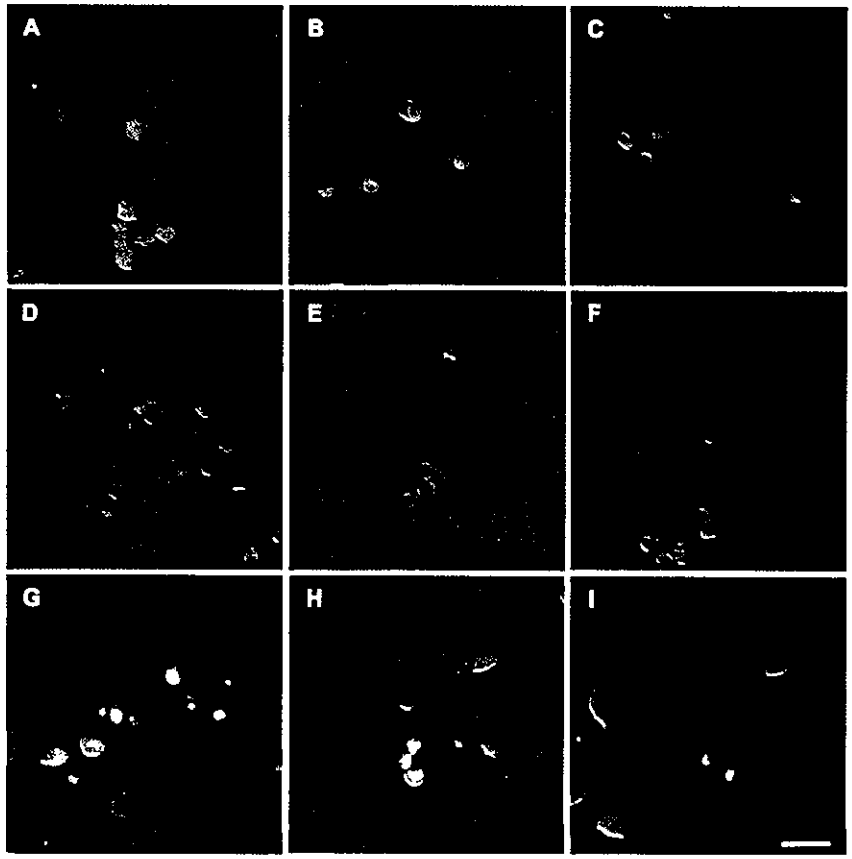

FIG. 7. **TUNEL assay.** Overlays of two images were taken by laser confocal microscopy 48 h after transfection. *A*, Cyto-wtSOD1; *B*, Cyto-mSOD1^{G93A}; *C*, Cyto-mSOD1^{G85R}; *D*, Mito-wtSOD1; *E*, Mito-mSOD1^{G93A}; *F*, Mito-mSOD1^{G85R}; *G–I*, EGFP-LacZ transfected cells incubated with 0.01 μM staurosporin for 24 h as positive controls (red nuclear staining in pycnotic cells). The cells with Cyto-mSOD1 (*B* and *C*) or Mito-SOD1 (*E* and *F*) showed negative staining as well as those with wtSOD1 (*A* and *D*). *Scale bar*, 30 μm.

a pathogenic process (30), although this has been disputed (31–33, 35). In this study, we conclusively demonstrated that cytoplasmic aggregates are not directly associated with cell death, similar to the *in vivo* models of polyglutamine diseases, suggesting that the subcellular localization of mutant protein itself, rather than aggregate formation, exerts toxicity (14, 30).

Controversy surrounds the issue of whether the motor neuronal cell death in mutant SOD1-associated FALS is apoptosis (47, 48) or not (49). A previous study on an *in vivo* model reported that activated caspase-3-positive motor neurons were observed, but TUNEL-positive motor neurons were not (43). Similarly, we were unable to find TUNEL-positive cells despite obvious activation of caspase-3. Recently, at least three types of programmed cell death (PCD) have been proposed: apoptosis, apoptosis-like PCD, and necrosis-like PCD (50). Apoptosis-like PCD is cell death with less chromatin condensation than in apoptosis or any degree and combination of apoptotic features such as caspase activation, cytoplasmic shrinkage, and plasma membrane blebbing (50). Previous reports suggested that apoptosis-like PCD may be a type of neuronal cell death in neurodegenerative diseases including ALS (51, 52). The present study also indicated the possibility that this apoptosis-like PCD is a type of neuronal cell death through the mitochondrial signal pathway in motor neurons with mutant SOD1. However, further investigations are needed to shed light on the mechanism of mutant SOD1-mediated neuronal cell death.

In conclusion, in this study we demonstrated that mitochondrial localization of mutant SOD1 itself triggers cytochrome *c* release from the mitochondria into the cytosol that initiates the caspase-dependent cell death cascade in a FALS model. Inhibition of mitochondrial localization of mutant SOD1 may well be a candidate for a therapeutic approach to FALS.

Acknowledgments—We are grateful to Dr. Keiji Tanaka (Department of Molecular Oncology, The Tokyo Metropolitan Institute of Medical Science) and Dr. Jun-ichi Niwa (Department of Neurology, Nagoya University Graduate School of Medicine) for helpful discussion. We also thank Dr. Kumi Kawai (Department of Pathology, Nagoya University Graduate School of Medicine) for technical assistance.

REFERENCES

1. Rosen, D. R., Siddique, T., Patterson, D., Figlewicz, D. A., Sapp, P., Hentati, A., Donaldson, D., Goto, J., O'Regan, J. P., Deng, H. X., Rahmani, Z., Krizus, A., McKenna-Yasek, D., Cayabyab, A., Gaston, S. M., Berger, R., Tanzi, R. E., Halperin, J. J., Herzfeldt, B., den Bergh, R. V., Hung, W. Y., Bird, T., Deng, G., Mulder, D. W., Smyth, C., Laing, N. G., Soriano, E., Pericak-Vance, M. A., Haines, J., Rouleau, G. A., Gusella, J. S., Horvitz, H. R., and Brown, R. H. (1993) *Nature* **362,** 59–62
2. Hirano, A. (1996) *Neurology* **47,** (Suppl. 2) S63–S66
3. Yim, M. B., Kang, J. H., Yim, H. S., Kwak, H. S., Chock, P. B., and Stadtman, E. R. (1996) *Proc. Natl. Acad. Sci. U. S. A.* **93,** 5709–5714
4. Wong, P. C., Pardo, C. A., Borchelt, D. R., Lee, M. K., Copeland, N. G., Jenkins, N. A., Sisodia, S. S., Cleveland, D. W., and Price, D. L. (1995) *Neuron* **14,** 1105–1116
5. Dal Canto, M. C., and Gurney, M. E. (1994) *Am. J. Pathol.* **145,** 1271–1279
6. Shibata, N., Hirano, A., Kobayashi, M., Siddique, T., Deng, H. X., Hung, W. Y., Kato, T., and Asayama, K. (1996) *J. Neuropathol. Exp. Neurol.* **55,** 481–490
7. Shibata, N., Hirano, A., Kobayashi, M., Dal Canto, M. C., Gurney, M. E., Komori, T., Umahara, T., and Asayama, K. (1998) *Acta Neuropathol.* **95,** 136–142
8. Kong, J., and Xu, Z. (1998) *J. Neurosci.* **18,** 3241–3250
9. Jaarsma, D., Haasdijk, E. D., Grashorn, J. A. C., Hawkins, R., van Duijn, W., Verspaget, H. W., London, J., and Holstege, J. C. (2000) *Neurobiol. Dis.* **7,** 623–643
10. Klement, I. A., Skinner, P. J., Kaytor, M. D., Yi, H., Hersch, S. M., Clark, H. B., Zoghbi, H. Y., and Orr, H. T. (1998) *Cell* **95,** 41–53
11. Saudou, F., Finkbeiner, S., Devys, D., and Greenberg, M. E. (1998) *Cell* **95,** 55–66
12. Schilling, G., Wood, J. D., Duan, K., Slunt, H. H., Gonzales, V., Yamada, M., Cooper, J. K., Margolis, R. L., Jenkins, N. A., Copeland, N. G., Takahashi, H., Tsuji, S., Price, D. L., Borchelt, D. R., and Ross, C. A. (1999) *Neuron* **24,** 275–286
13. Kobayashi, Y., Kume, A., Li, M., Doyu, M., Hata, M., Ohtsuka, K., and Sobue, G. (2000) *J. Biol. Chem.* **275,** 8772–8778
14. Katsuno, M., Adachi, H., Kume, A., Li, M., Nakagomi, Y., Niwa, H., Sang C., Kobayashi, Y., Doyu, M., and Sobue, G. (2002) *Neuron* **35,** 843–854
15. Mattson, M. P., Guo, Q., Furukawa, K., and Pedersen, W. A. (1998) *J. Neurochem.* **70,** 1–14
16. Katayama, T., Imaizumi, K., Honda, A., Yoneda, T., Kudo, T., Takeda, M., Mori, K., Rozmahel, R., Fraser, P., George-Hyslop, P. S., and Tohyama, M. (2001) *J. Biol. Chem.* **276,** 43446–43454
17. Imai, Y., Soda, M., Inoue, H., Hattori, N., Mizuno, Y., and Takahashi, R. (2001) *Cell* **105,** 891–902
18. Carrì, M. T., Ferri, A., Battistoni, A., Famhy, L., Gabbianelli, R., Poccia, F., and Rotilio, G. (1997) *FEBS Lett.* **414,** 365–368
19. Beal, M. F. (2000) *Brain* **123,** 1291–1292
20. Guégan, C., Vila, M., Rosoklija, G., Hays, A. P., and Przedborski, S. (2001) *J. Neurosci.* **21,** 6569–6576
21. Zhu, S., Stavrovskaya, I. G., Drozda, M., Kim, B. Y., Ona, V., Li, M., Sarang, S., Liu, A. S., Hartley, D. M., Wu, D. C., Gullans, S., Ferrante, R. J., Przedborski, S., Kristal, B. S., and Friedlander, R. M. (2002) *Nature* **417,** 74–78
22. Menzies, F. M., Cookson, M. R., Taylor, R. W., Turnbull, D. M., Chrzanowska-Lightowlers, Z. M., Dong, L., Figlewicz, D. A., and Shaw, P. J. (2002) *Brain* **125,** 1522–1533
23. Mattiazzi, M., D'Aurelio, M., Gajewski, C. D., Martushova, K., Kiaei, M., Beal, M. F., and Manfredi, G. (2002) *J. Biol. Chem.* **277,** 29626–29633
24. Yoshihara, T., Ishigaki, S., Yamamoto, M., Liang, Y., Niwa, J., Takeuchi, H., Doyu, M., and Sobue, G. (2002) *J. Neurochem.* **80,** 158–167
25. Ishigaki, S., Liang, Y., Yamamoto, M., Niwa, J., Ando, Y., Yoshihara, T., Takeuchi, H., Doyu, M., and Sobue, G. (2002) *J. Neurochem.* **82,** 576–584
26. Menzius, F. M., Ince, P. G., and Shaw, P. J. (2002) *Neurochem. Int.* **40,** 543–551
27. Sturtz, L. A., Diekert, K., Jensen, L. T., Lill, R., and Culotta, V. C. (2001) *J. Biol. Chem.* **276,** 38084–38089
28. Jaarsma, D., Rognoni, F., van Duijn, W., Verspaget, H. W., Haasdijk, E. D., and Holstege, J. C. (2001) *Acta Neuropathol.* **102,** 293–305
29. Higgins, C. M., Jung, C., Ding, H., and Xu, Z. (2002) *J. Neurosci.* **22,** RC215
30. Bruijin, L. I., Houseweart, M. K., Kato, S., Anderson, K. L., Anderson, S. D., Ohama, E., Reaume, A. G., Scott, R. W., and Cleveland, D. W. (1998) *Science* **281,** 1851–1854
31. Cummings, C. J., Reinstein, E., Sun, Y., Antalffy, B., Jiang, Y., Ciechanover, A., Orr, H. T., Beaudet, A. L., and Zoghbi, H. Y. (1999) *Neuron* **24,** 879–892
32. Johnston, J. A., Dalton, M. J., Gurney, M. E., and Kopito, R. R. (2000) *Proc. Natl. Acad. Sci. U. S. A.* **97,** 12571–12576
33. Kopito, R. R. (2000) *Trends Cell Biol.* **10,** 524–530
34. Bruening, W., Roy, J., Giasson, B., Figlewicz, D. A., Mushynski, W. E., and Durham, H. D. (1999) *J. Neurochem.* **72,** 693–699
35. Takeuchi, H., Kobayashi, Y., Yoshihara, T., Niwa, J., Doyu, M., Ohtsuka, K., and Sobue, G. (2002) *Brain Res.* **949,** 11–22
36. Wang, J., Xu, G., and Borchelt, D. R. (2002) *Neurobiol. Dis.* **9,** 139–148
37. Matsuyama, S., and Reed, J. C. (2000) *Cell Death. Differ.* **7,** 1155–1165
38. Gupta, S. (2001) *Life Sci.* **69,** 2957–2964
39. Green, D. R., and Reed, J. C. (1998) *Science* **281,** 1309–1312
40. Adams, J. M., and Cory, S, (1998) *Science* **281,** 1322–1326
41. Lee, M. H., Hyun, D.-H., Halliwell, B., and Jenner, P. (2001) *J. Neurochem.* **78,** 209–220
42. Li, M., Ona, V. O., Guégan, C., Chen, M., Jackson-Lewis, V., Andrews, L. J., Olszewski, A. J., Stieg, P. E., Lee, J.-P., Przedborski, S., and Friedlander, R. M. (2000) *Science* **288,** 335–339
43. Pasinelli, P., Houseweart, M. K., Brown, R. H., Jr., and Cleveland, D. W. (2000) *Proc. Natl. Acad. Sci. U. S. A.* **97,** 13901–13906
44. Wang, N., Gottesman, S., Willingham, M. C., Gottesman, M. M., and Maurizi, M. R. (1993) *Proc. Natl. Acad. Sci. U. S. A.* **90,** 11247–11251
45. Wang, N., Maurizi, M. R., Emmert-Buck, L., and Gottesman, M. M. (1994) *J. Biol. Chem.* **269,** 29308–29313
46. Okado-Matsumoto, A., and Fridovich, I. (2002) *Proc. Natl. Acad. Sci. U. S. A.* **99,** 9010–9014
47. Durham, H. D., Roy, J., Dong, L., and Figlewicz, D. A. (1997) *J. Neuropathol. Exp. Neurol.* **56,** 523–530
48. Martin, L. J. (1999) *J. Neuropathol. Exp. Neurol.* **58,** 459–471
49. Bendotti, C., Calvaresi, N., Chiveri, L., Prelle, A., Moggio, M., Braga, M., Silani, V., and De Biasi, S. (2001) *J. Neurol. Sci.* **191,** 25–33
50. Leist, M., and Jäättelä, M. (2001) *Nat. Rev. Mol. Cell. Biol.* **2,** 589–598
51. Turmaine, M., Raza, A., Mahal, A., Mangiarini, L., Bates, G. P., and Davies, S. W. (2000) *Proc. Natl. Acad. Sci. U. S. A.* **97,** 8093–8097
52. Sperandio, S., de Belle, I., and Bredesen, D. E. (2000) *Proc. Natl. Acad. Sci. U. S. A.* **97,** 14376–14381

Journal of Neurochemistry, 2002, 80, 158–167

Differential expression of inflammation- and apoptosis-related genes in spinal cords of a mutant SOD1 transgenic mouse model of familial amyotrophic lateral sclerosis

Tsuyoshi Yoshihara, Shinsuke Ishigaki, Masahiko Yamamoto, Yideng Liang, Jun-ichi Niwa, Hideyuki Takeuchi, Manabu Doyu and Gen Sobue

Department of Neurology, Nagoya University Graduate School of Medicine, Nagoya, Japan

Abstract

Familial amyotrophic lateral sclerosis (FALS)-linked mutations in copper–zinc superoxide dismutase (SOD1) cause motor neuron death through one or more acquired toxic properties. We analyzed the molecular mechanism underlying motor neuron degeneration in the transgenic mouse model expressing the SOD1 gene with G93A mutation. Using cDNA microarray, the differentially expressed genes were identified in the spinal cords of G93A mice, 30 being elevated and seven decreased. cDNA microarray analysis to monitor gene expression during neurodegeneration revealed an up-regulation of genes related to an inflammatory process, such as the tumor necrosis factor-α (TNF-α) gene, resulting from glial cell activation, together with the change in apoptosis-related gene expression, such as caspase-1. The increased expression of the inflammation- and apoptosis-related genes occurred at 11 weeks of age in the presymptomatic stage prior to motor neuron death. These results suggest a mechanism of neurodegeneration that includes an inflammatory response as an important component. Thus, ALS has paralleled other neurodegenerative disorders, such as Alzheimer's and prion diseases, in which the inflammatory process is believed to participate directly in neuronal death.

Keywords: amyotrophic lateral sclerosis (ALS), copper–zinc superoxide dismutase (SOD1), inflammation, microarray, neurodegeneration, spinal cord.

J. Neurochem. (2002) **80**, 158–167.

Amyotrophic lateral sclerosis (ALS) is a neurodegenerative disease characterized by the degeneration of motor neurons in the spinal cord, brain stem and motor cortex, resulting in paralysis of limb, bulbar and respiratory muscles (Haverkamp *et al.* 1995; Mitsumoto 1997). About 10% of ALS shows a familial trait, and 10–20% of these familial ALS (FALS) patients are caused by the missense mutations of Cu/Zn superoxide dismutase (SOD1) (Cudkowicz *et al.* 1997). Mice expressing human mutant SOD1 develop age-dependent ALS-like neurological symptoms and pathological features of motor neuron degeneration and cytoplasmic inclusions consisting of mutant SOD1 (Gurney *et al.* 1994; Brown 1995; Wong *et al.* 1995; Tu *et al.* 1996), providing a comprehensive model of human FALS with SOD1 mutation.

As knock-out mice lacking endogenous SOD1 fail to show motor neuron degeneration (Reaume *et al.* 1996), a toxic gain-of-function of mutant SOD1 has been considered to be a cause of neurodegeneration in the transgenic mice expressing mutant SOD1. The molecular mechanism underlying this toxic gain-of-function, which induces motor neuron degeneration, however, remains unknown. Several lines of evidence suggest that oxidative stress is one of the causes of motor neuron degeneration with mutant SOD1. *In vitro* studies revealed an increased affinity of mutant SOD1 for hydrogen peroxide resulting in enhanced hydroxyl radical formation (Yim *et al.* 1996). Protein carbonylation, lipid peroxidation and free protein-bound 3-nitrotyrosine levels are also markedly increased in the spinal cords of ALS patients (Beal *et al.* 1997; Ferrante *et al.* 1997; Pedersen *et al.* 1998). On the other hand, neuronal apoptosis has been

Received July 9, 2001; revised manuscript received October 2, 2001; accepted October 10, 2001.

Address correspondence and reprint requests to Dr Gen Sobue, Department of Neurology, Nagoya University Graduate School of Medicine, Nagoya 466, Japan. E-mail: sobueg@tsuru.med.nagoya-u.ac.jp

Abbreviations used: ALS, amyotrophic lateral sclerosis; FALS, familial amyotrophic lateral sclerosis; SDS, sodium dodecyl sulfate; SOD1, copper–zinc superoxide dismutase; SSC, saline sodium citrate buffer; TNF-α, tumor necrosis factor-α, xiap, X-chromosome-linked inhibitor of apoptosis.

suggested to underlie the neurodegeneration of motor neurons with mutant SOD1 expression. The activation of caspase-1 and caspase-3 in the spinal cord has been shown in G93A-SOD1 mice and, interestingly, treatment with a broad caspase inhibitor delayed disease onset (Li *et al.* 2000; Pasinelli *et al.* 2000). The activation of caspase-1 is an most early event in motor neuron death in several types of mutant SOD1 mice. Moreover, neuronal apoptosis has been demonstrated to underlie several neurodegenerative diseases including Alzheimer's disease (Lassmann *et al.* 1995; Stadelmann *et al.* 1999), prion diseases (Gray *et al.* 1999) and HIV-dementia (Gray *et al.* 2000).

In neuronal degeneration, a significant inflammatory process involving microglial and astroglial activation has been documented to parallel it, and this inflammatory process potently produces neurotoxic cytokines, proteases, small reactive cytotoxic molecules and oxyradicals (Minghetti and Levi 1998). Although the inflammatory process has been considered to be a secondary event following the primary neuronal degeneration, this process can enhance neuronal degeneration through the production of these molecules. Caspase-1 itself is involved in the apoptosis process, and several recent evidences suggest that caspase-1 activation also enhances the inflammatory response (Li *et al.* 2000). Furthermore, the inflammatory process is important from the therapeutic point of view, as the neurodegeneration could be ameliorated by inhibiting the inflammatory-related events. Indeed, the inflammatory cytokines and caspases were reported to increase in the serum and lesioned tissues of human ALS and its transgenic models (Li *et al.* 2000; Pasinelli *et al.* 2000; Poloni *et al.* 2000), while the information is restricted to certain selected cytokines and apoptosis-related molecules.

We now demonstrate that a wide variety of inflammation- and apoptosis-related genes are differentially expressed in the process of neurodegeneration in the G93A-SOD1 mice spinal cord using microarray and macroarray analyses confirmed by RT-PCR analysis. The results support the view that the inflammatory process is a pivotal factor in developing motor neuron degeneration and causing motor neuron death in FALS.

Materials and methods

Transgenic mice

Transgenic mice expressing the human SOD1 gene with a G93A mutation (Gurney *et al.* 1994) were purchased from the Jackson Laboratory (Bar Harbor, ME, USA) and maintained as hemizygotes by mating transgenic males with B6/SJLF1 females. Non-transgenic littermates were used as controls.

Microarray analysis

Pooled mRNA samples were obtained from the lumbar spinal cords (L1-L5) of three to five G93A-SOD1 mice at 7 ($n = 3$), 11 ($n = 4$), 14 ($n = 5$) and 17 ($n = 4$) weeks of age, and of four non-transgenic littermates each at the same age. All mice were killed under deep anesthesia with ether. Total RNA was purified with Micro RNA Isolation Kit (Stratagene, San Diego, CA, USA). Total RNA samples (5 μg) from the G93A-SOD1 mice and non-transgenic littermates were reverse transcribed into first-strand cDNA, using 20 U Superscript II (Life Technologies, Rockville, MD, USA) and 1 μL of 0.5 mg/mL T7-oligo-dT primer (5′-TCTAGTCGACG-GCCAGTGAATTGTAATACGACTCACTATAGGGCGT$_{21}$–3′), at 42°C for 1 h in 20 μL of reaction [1 × first-strand reaction buffer, 10 mM DTT, 0.25 mM dNTPs, 20 U RNasin (Promega, Madison, WI, USA)]. Next, 30 μL of 5 × second-strand synthesis buffer, 3 μL of 10 mM dNTPs, 4 μL DNA polymerase I, 1 μL *Escherichia coli* RNase H, 1 μL E. coli DNA ligase and 92 μL of RNase-free H_2O were added, incubated at 16°C for 2 h, then incubated at 16°C for 10 min after the addition of 2 μL of T4 DNA polymerase. The double-stranded cDNA was extracted with 150 μL of phenol–chloroform to get rid of proteins and purified using a Microcon-100 column to separate out the unincorporated nucleotides and salts. The RNA amplification was performed using Ampliscribe T7 Transcription Kit (Epicentre Technologies, Madison, WI, USA) in a mixture of 8 μL double-stranded cDNA, 2 μL of 10 × Ampliscribe T7 buffer, 1.5 μL each of 100 mM ATP, CTP, GTP and UTP, 2 μL 0.1 M DTT and 2 μL of T7 RNA polymerase, which were incubated at 42°C for 3 h. The amplified RNA was purified with RNeasy Mini Kits (Qiagen, Valencia, CA, USA). T7 RNA polymerase-amplified RNA (aRNA) was labeled with Cy3 and Cy5 fluorescent dyes, respectively, using Atlas Glass Fluorescent Labeling Kit (Clontech, Palo Alto, CA, USA). Cy3- and Cy5-labeled probes were hybridized to mouse Atlas Glass microarrays (Clontech) at 50°C for 16 h. This microarray includes 1081 genes with various functional categories proportionally, such as the genes related to oncogenes and tumor suppressors, cellular signaling, apoptosis, and transcription regulators. The microarrays were washed according to the manufacturer's instructions, the slides were air-blown dried, prepared for scanning, and scanned for fluorescence with GenePix (Axon, Union City, CA, USA).

Macroarray analysis

The double-stranded cDNA was labeled with digoxigenin (DIG) using T7 RNA polymerase amplification. Ampliscribe T7 Transcription Kit (Epicentre Technologies) was applied for RNA amplification. The mixture of 6.55 μL double-stranded cDNA, 2.5 μL of 10 × Ampliscribe T7 buffer, 1.5 μL each of 100 mM ATP, CTP and GTP, 1.45 μL of 100 mM UTP, 5 μL DIG RNA labeling mix (Roche Molecular Biochemicals, Indianapolis, IN, USA), 2.5 μL of 0.1 M DTT and 2.5 μL of T7 RNA polymerase were incubated at 42°C for 3 h. The amplified RNA was purified with RNeasy Mini Kits (QiaGen). DIG-labeled aRNA was hybridized to mouse Atlas Array 1.2 (Clontech), which contains 1176 mouse cDNA with various functional categories as shown in the microarray, at 50°C for 16 h in the solution of 50% formamide, 5 × saline sodium citrate buffer (SSC), 5% sodium dodecyl sulfate (SDS) and 2% blocking reagent (Roche Diagnostics). After hybridization, the array was washed three times at 65°C for 30 min in 0.1 × SSC and 0.1% SDS. Immunological detection was performed following the procedure of Engler-Blum *et al.* (1993). The array was incubated in blocking buffer (0.5% blocking reagent and 3 M NaCl in 0.1 M phosphate buffer) at room temperature for 60 min, followed by the

reaction with anti-DIG-alkaline phosphatase conjugate (1 : 20 000). The array was reacted with 0.2 mM CDPstar for 10 min, and then exposed to X-ray film for 5–30 min.

Semi-quantitative RT-PCR analysis

The semiquantitative mRNA expression levels were determined by using a QuantumRNA β-actin Internal Standard Kit (Ambion Inc, Austin, TX, USA) that is essentially based on relative multiplex RT-PCR with β-actin Competimers. cDNA was synthesized from total RNA by reverse transcriptase reaction with Superscript II (Life Technologies). cDNA synthesized from 10 ng of total RNA was used as template for PCR amplification in each reaction. The primer sets used for these assays are shown in Table 1. PCR amplification was performed with AmpliTaq Gold (Perkin-Elmer). The appropriate number of PCR cycles for each specific cDNA was determined in the linear range of cycles prior to onset of the plateau. The linear relationship between the amount of the template and the PCR product was also ascertained with respect to cDNA input. The RT-PCR analysis was performed in duplicate samples from pooled mRNAs. Amplified cDNA was detected by ethidium bromide staining and quantified with a Gel Doc 2000 (Bio-Rad Laboratories, Hercules, CA, USA).

Table 1 Oligonucleotide primer for RT-PCR

Genes		Oligonucleotide
vimentin	Forward	TGCCCTTGAAGCTGCTAACTAC
	Reverse	CAACCAGAGGAAGTGCATCCAG
cathepsin D	Forward	GTGGAAAGACAATCTGCCTGAG
	Reverse	TGGCTTCCTCTACTGGACTCTG
c-fos	Forward	GAATGGTGAAGACCGTGTCAG
	Reverse	CTGCAACGCAGACTTCTCATC
xiap	Forward	ACAGTGTGCAGAAGCAGTTGAC
	Reverse	TGTTAGCATTGGTCTCCATTTG
GABAA-R	Forward	CGACCGACTGTCAAGAATAGC
	Reverse	AGGAATCACTGCGTTGAGAAC
TNF-α	Forward	AGCCGATTTGCTATCTCATACC
	Reverse	AGTACTTGGGCAGATTGACCTC
CD68	Forward	CCGAATCCTATACCCAATTCAG
	Reverse	AGCAGCCTGTAGCCTTAGAGAG
SPI2-4	Forward	ACCAGAGACCCTGAGGAAATG
	Reverse	GAGACACACTCAGGTCCTTGG
CD147	Forward	CCTGAGAAGTCACAGCTGACC
	Reverse	GGATGGGATACTGGAGTGGAG
GFAP	Forward	AACAATTCAGACAGAAAGGGAAAG
	Reverse	TCAGTTCCTCAAACTCTCAAATAGG
JunD	Forward	CCAGTACGCAGTTCCTCTACC
	Reverse	ACTGCTCAGGTTGGCGTAGAC
JAK3	Forward	TACATCTCTTTGCTGGGCAAG
	Reverse	CGGTACTTGACGATGAAGTCG
clusterin	Forward	GTCACTGAGGTGGTGGTGAAG
	Reverse	GAGATTCCCTCCCAGACACTC
Bcl-xL	Forward	TGAATGAACTCTTTCGGGATG
	Reverse	GATCCAAGGCTCTAGGTGGTC
caspase-1	Forward	TGGTCTTGTGACTTGGAGGA
	Reverse	TGGCTTCTTATTGGCACGAT

Immunohistochemistry

Three to five mutant SOD1 mice and age-matched littermate mice at 7, 11, 14 and 17 weeks of age were used for the pathologic analysis. The mice were perfused with 10% buffered formalin and the lumbar spinal cord was removed. Four micrometer thick sequential transverse sections of the spinal cords were made from each mouse and processed for embedding in paraffin. Selected sections were stained with hematoxylin and eosin, and the neighboring sections were used for immunostaining. The deparaffinized and rehydrated sections were treated with trypsin and then were incubated with anti-cathepsin D, anti-vimentin and anti-TNFα antibodies (Santa Cruz Biotechnology, Santa Cruz, CA, USA) overnight at 4°C as described previously (Yamamoto *et al.* 2001). The washed sections were incubated with biotinylated anti-rabbit Ig or anti-rat Ig antibody (Dako, Carrinteria, CA, USA) and subsequently with streptavidin-peroxidase complex. Sections were incubated with peroxidase-labeled goat anti-mouse IgG antibody (Sigma, St Louis, MO, USA) for phosphotyrosine detection. The peroxidase reaction was visualized with diaminobenzidine and hydrogen peroxide.

In situ hybridization analysis

In situ hybridization for xiap mRNA was performed as described previously (Mitsuma *et al.* 1999; Ishigaki *et al.* 2000). Spinal cord tissues were embedded in OCT compound (Sakura Finetek, Torrance, CA, USA) and quickly frozen in liquid nitrogen. Ten μm-thick frozen sections were prepared with a cryostat. For making probes, xiap was PCR-amplified with the oligonucleotide primers (forward: 5′-GGAATCTTTGGGAAGAACTGC-3′ and reverse: 5′-TTGTCAACTGCTTCTGCACAC-3′). The PCR products were ligated into the expression plasmid vector and transformed into competent *E. coli* cells. DIG-labeled antisense cRNA probe of 400 bp was generated for *in situ* hybridization from linearized plasmids for xiap, using T7 polymerase (Roche Diagnostics). Control sense probe was generated using SP6 RNA polymerase. Sliced tissues were hybridized with these cRNA probes at 40°C for 16 h in the solution (50% formaldehyde, 10 mM Tris-HCl, pH 7.6, 1 mM EDTA, pH 8.0, 0.6 M NaCl, 0.25% SDS, 0.1 mg/mL yeast tRNA, 10% dextran sulfate, and 1 × Denhardt's solution). Next, the slides were washed at room temperature in formamide/1 × SSC (1 : 1), then at 50°C for 30 min in 1 × SSC. The signals were detected immunologically with alkaline phosphatase-conjugated anti-DIG antibody according to the manufacturer's protocol (Roche Diagnostics).

Results

Mutual confirmation of mRNA expression levels in microarray, macroarray and RT-PCR analyses

We demonstrated gene expression profiles of several selected genes, which markedly altered their expression levels in the spinal cords between mutant SOD1 mice and littermate control mice in microarray, macroarray and RT-PCR analyses (Figs 1a–c). The gene expression levels determined by these three analyses were well correlated with each other (Fig. 1d), indicating that the expression levels quantified by these methods were validated. We further studied the temporal

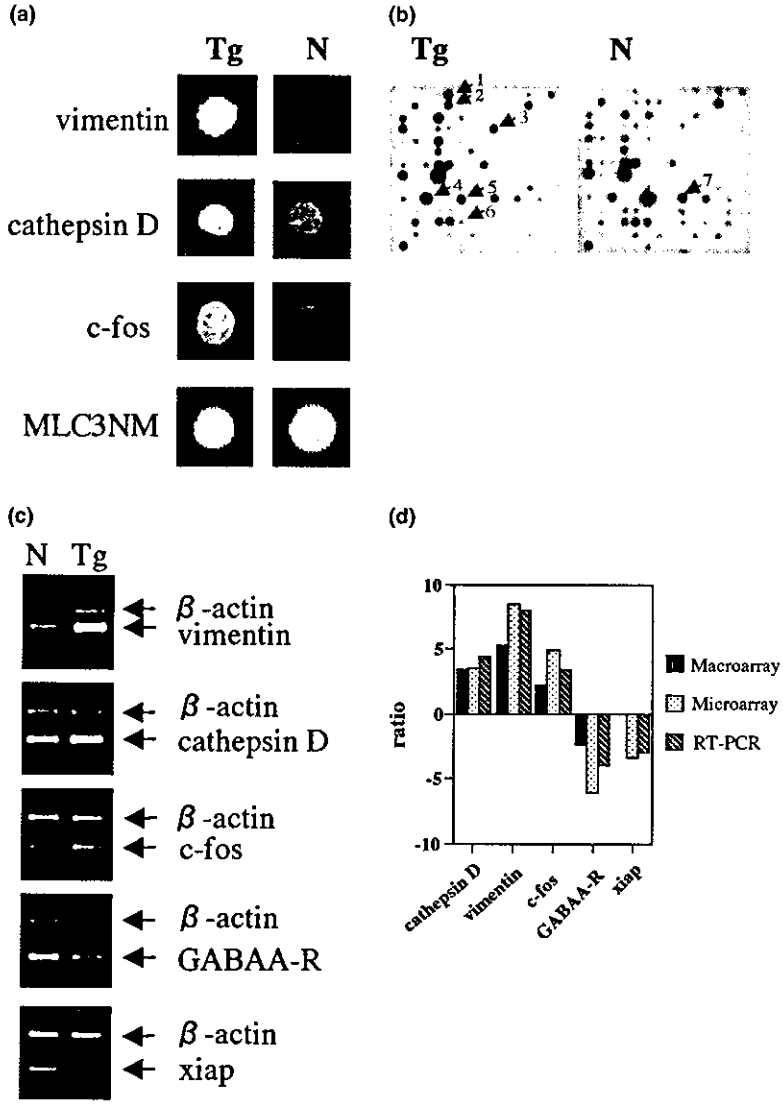

Fig. 1 Gene expression and mutual confirmation of expression levels in microarray, macroarray and RT-PCR analyses. Close-up images of microarray (a) and macroarray (b) are shown. In microarray analysis (a), the expressions of vimentin, cathepsin D and c-fos genes are up-regulated but the non-muscle myosin light chain 3 (MLC3NM) expression is not changed in mutant SOD1 mice (mSOD-Tg) compared with those in wt normal littermate mice (*n*), at 17 weeks of age. In the macroarray (b), arrows indicate several genes differentially expressed, serine protease inhibitor 2–2 (1), serine protease inhibitor 2–4 (2), vimentin (3), cathepsin D (4), neurofilament-L (5) and neurofilament-M (6). The MLC3NM gene (7) expression was not altered in the macroarray as well as in the microarray. The vimentin, cathepsin D and c-fos expression levels are elevated in mutant SOD1 mice with the RT-PCR analysis, whereas the GABAA-R and xiap expression levels are decreased (c). The levels of gene expression were standardized against that of β-actin as an internal control. A good correlation of the expression ratios of the standardized values of mutant SOD1 against control mice, the positive and negative ratios of which indicate the increase and decrease of gene expression in mutant SOD1 mice compared with controls, was obtained among these three methods as shown in (d).

expression pattern of the differential genes (Figs 2 and 3), together with the localization of the gene expression selected (Fig. 4).

Gene expression profiles in the spinal cords of G93A SOD1 mice

Thirty genes expressed more than 3.0-fold mRNA levels in the spinal cords of the 17-week-old G93A-SOD1 mice, as compared with those of the littermates on microarray analysis (Table 2). Only seven genes were differentially down-regulated in mutant SOD1 mice by 0.3-fold or less at 17 weeks of age. The up-regulated genes are characterized by the inflammatory process-related genes. In the highly expressed genes in mutant SOD1 mice, vimentin, TNF-α, p-selectin glycoprotein ligand 1, CD147, junD1, cathepsin D, CD68, preproenkephalin 2, serine protease inhibitor 2–4 (SPI 2–4) and cystatin C precursor genes are the inflammatory process-related genes, which have been reported to be up-regulated in brain ischemia (Palm *et al.* 1995; Kamme and Wieloch 1996; Vartiainen *et al.* 1996; Cui *et al.* 1999; Friedman *et al.* 2000), traumatic brain injury (Hill *et al.* 1996; Lu *et al.* 2000) and demyelinating diseases like multiple sclerosis (Bitsch *et al.* 1998). CD147 and CD68 are expressed by the macrophage/microglia lineage (Inoue *et al.* 1999). Bcl2L1 (Bcl-xL) and caspase-1 genes are known to be involved in the apoptotic process. On the other hand, anti-apoptotic protein (Deveraux *et al.* 1997; Datta *et al.* 2000), X-chromosome-linked inhibitor of apoptosis (xiap) expression level was markedly decreased in mutant SOD1 mice at 17 weeks of age. The genes of growth factors and transcriptional regulators were up- or down-regulated independently. In addition to these genes, the transcripts for retinoid X receptor α and homeobox proteins were up-regulated in mutant SOD1 mice.

As for the temporal profile of gene expression, there was a marked differential temporal pattern (Figs 2 and 3, Table 2).

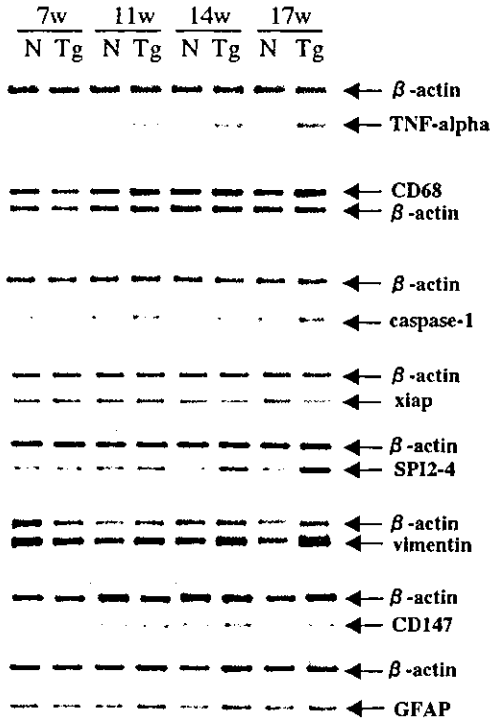

Fig. 2 Chronological RT-PCR analysis of differential gene expression in spinal cords. Representative results of the RT-PCR analysis for the target and β-actin transcripts are shown. The RT-PCR analysis was performed in mutant SOD1 transgenic (Tg) and normal littermate (N) mice at 7, 11, 14 and 17 weeks, as described in the text.

Among the inflammation-related genes, the TNF-α, CD68, and JAK3 genes were significantly increased in their expression at 11 weeks of age, and further elevated at 14 and 17 weeks (Fig. 3). The vimentin, SPI 2–4, cathepsin D, CD147, glial fibrillary acidic protein (GFAP) and clusterin gene expression was not significantly elevated at 11 weeks but greatly elevated at 14 and 17 weeks (Fig. 3). In the apoptosis-related genes, the caspase-1 gene expression was markedly increased in 11 weeks and reached a plateau thereafter. The Bcl-xL gene expression level was not elevated at 11 weeks of age but was highly increased by 14 and 17 weeks (Fig. 3). The xiap gene expression was maintained until 11 weeks of age, and gradually decreased to 0.6-fold in 14 weeks and to 0.3-fold in 17 weeks (Fig. 3). The GABAA-R gene was stably expressed from 7 through 14 weeks, but drastically declined to 0.3-fold in 17-week-old-mutant mice. In the transcription factors, c-Fos and JunD of the Jun family proto-oncogenes increased their expression at 17 weeks of age in the terminal stage. At 7 weeks of age, there were no significant alterations in expression levels in mutant SOD1 mice.

Immunohistochemistry and *in situ* hybridization

Cathepsin D immunoreactivity was detected mainly in motor neurons and weakly in glial cells in control littermates, but it was strongly detected in astrocytes and invading microglia in 14- and 17-week-old mutant SOD1 mice (Figs 4a and b). Strikingly, cathepsin D was also present in the remaining motor neurons of mutant SOD1 mice at 17 weeks of age. Immunoreactivity of vimentin was not observed in the littermate mice, whereas it was detected to a high degree in astrocytes and microglia in 17-week-old mutant SOD1 mice (Figs 4c and d). Furthermore, TNF-α immunoreactivity was not demonstrated at 7 weeks of age in mutant SOD1 mice or in littermates. It was intensely detectable from 11 through 17 weeks of age particularly in invading microglia of mutant SOD1 mice, and motor neurons were also immunoreactive for TNF-α (Figs 4e and f).

In situ hybridization of the xiap gene showed strong signals in the cytoplasm of motor neurons and glial cells, especially in astrocytes in the littermate mice (Figs 4h and j). In mutant SOD1 mice, the hybridization signals were significantly decreased in motor neurons as well as in glial cells at 14 and 17 weeks of age (Figs 4g and i), indicating that the expression levels per individual neuron and glial cell were diminished in mutant SOD1 mice.

Discussion

In this study, we have isolated a number of transcripts with a significant differential expression in the lumbar spinal cord of mutant SOD1 mice compared with littermate controls. To screen a large number of transcripts in the spinal cords, we have hybridized high-density cDNA in micro- and macro-array with labeled mRNA of the spinal cords from mutant SOD1 and control mice. The sensitivity and specificity of array technology were confirmed by RT-PCR analysis. Using mutant SOD1 mice as a mouse model of human FALS, we studied temporal and differential gene expression in spinal cords in relation to motor neuron degeneration and loss on disease progression. Before 11 weeks of age mutant SOD1 mice are free of a disease phenotype, but they begin to decline rapidly in motor function after 14 weeks of age, culminating in a moribund condition by 18 weeks.

The members of genes expressed highly in the spinal cords of mutant SOD1 mice suggested an inflammatory response with activated microglia and reactive astrocytes. The marked up-regulated genes expressed in mutant SOD1 mice included the genes of proteases and their inhibitors: cathepsin D, serine protease inhibitor 2–4 (SPI 2–4) and cystatin C precursor. The differential genes were expressed predominantly in the cell types: CD68, CD147 and p-selectin glycoprotein ligand 1 in microglia, and clusterin in astrocytes. The alteration of the cytoskeletal protein gene expression could reflect the number of motor neurons and glial cells during disease progression; the genes of neurofilaments were down-regulated but those of vimentin and GFAP were up-regulated. The gene expression of JAK3, which is a necessary component of cytokine receptor